Causal evidence for a domain-specific role of left superior frontal sulcus in human perceptual decision making

Miguel Barretto García,[1,2†] Marcus Grueschow,[1†] Marius Moisa,[1] Rafael Polania,[3] Christian C. Ruff[1]

[†] These authors contributed equally to this paper.

Affiliations:

[1] Zurich Center for Neuroeconomics (ZNE), Department of Economics, University of Zurich, Zurich, Switzerland.

[2] Department of Neuroscience, Washington University in St. Louis, Missouri, United States.

[3] Decision Neuroscience Lab, Department of Health Sciences and Technology, ETH Zurich, Zurich, Switzerland.

ABSTRACT

Humans and animals can flexibly choose their actions based on different information, ranging from objective states of the environment (e.g., apples are bigger than cherries) to subjective preferences (e.g., cherries are tastier than apples). Whether the brain instantiates these different choices by recruiting either specialised or shared neural circuitry remains debated. Specifically, domain-general accounts of prefrontal cortex (PFC) function propose that prefrontal areas flexibly process either perceptual or value-based evidence depending on what is required for the present choice, whereas domain-specific theories posit that PFC sub-areas, such as the left superior frontal sulcus (SFS), selectively integrate evidence relevant for perceptual decisions. Here we comprehensively test the functional role of the left SFS for choices based on perceptual and value-based evidence, by combining fMRI with a behavioural paradigm, computational modelling, and transcranial magnetic stimulation. Confirming predictions by a sequential sampling model, we show that TMS-induced excitability reduction of the left SFS selectively changes the processing of decision-relevant perceptual information and associated neural processes. In contrast, value-based decision making and associated neural processes remain unaffected. This specificity of SFS function is evident at all levels of analysis (behavioural, computational, and neural, including functional connectivity), demonstrating that the left SFS causally contributes to evidence integration for perceptual but not value-based decisions.

INTRODUCTION

Humans and animals alike perform a mélange of goal-directed decisions that require the accumulation of different types of information. If the goal, for example, is to accurately determine whether an apple is bigger than a cherry (perceptual choice), the decision-maker accumulates size information of each fruit; or, the decision-maker may draw out information from personal taste profiles if the goal is to determine whether consuming a cherry over an apple maximises their subjective preferences (value-based choice). Previous studies have shown that different brain circuitries are recruited to accumulate evidence that would instantiate such distinct goal-directed decisions (Summerfield and Tsetsos, 2012; Polanía et al., 2014, 2015; Grueschow et al., 2015); thus, it remains debated to what degree certain decision-making processes share neural circuitry or whether these processes operate under specialised systems. However, prior studies were largely correlational (Heekeren et al. 2004, 2008; Polanía et al., 2014; Grueschow et al., 2015), and most causal studies were only limited to one type of choice (Philiastides et al., 2011; Rahnev et al., 2016) and performed in animals (Ding and Gold, 2012b; Erlich et al., 2015; Hanks et al., 2015). Animal studies provide critical causal insights, yet direct translation to humans can be limited by species-specific anatomy and potential non-homologies (e.g., human SFS versus frontal orienting fields in rodents). Therefore, establishing causal contributions in the human brain remains essential.

In the absence of a comparison choice task, it is impossible to ascertain whether neural circuitry is domain-specific to a particular process, or domain-general that it may be involved across many types of choices. Very few studies (Polanía et al., 2014, 2015; Grueschow et al., 2015) have carefully matched perceptual and value-based decisions in terms of evidence strength, stimulus display, and response modality, and compare them through the lens of a common sequential-sampling framework of evidence accumulation (Dutilh and Rieskamp, 2016; Gold and Shadlen, 2007; Krajbich, 2019), which has long been applied to both perceptual (Ratcliff and Mckoon, 1988) as well as value-based (Busemeyer and Townsend, 1993; Usher and McClelland 2001) decisions. Such studies were able to identify common and specialised circuitries and mechanisms associated to perceptual or value-based decisions or both (Polanía et al., 2014; Grueschow et al., 2015).

But unless causality is established, it is even more difficult to attribute the circuitry's role in evidence accumulation for one or several choice domains, or whether its involvement is peripheral and merely functionally supporting a larger system. Given task complexity, such studies of observing causal neural effects in healthy human populations using non-invasive brain stimulation are incredibly sparse. One previous study has, at least, shown that causally de-synchronising frontoparietal connectivity specifically increased choice variability during value-based choice, but had no effect on perceptual decisions (Polanía et al., 2015); thus, establishing the causal role of the frontoparietal network during value-based choice. But while indeed causal, the study was limited, relative to the standards of evidence in animal studies (Erlich et al., 2015; Hanks et al., 2015; Piet et al., 2017), since its results, as in many causal stimulation studies in humans (Philiastides et al., 2011; Rahnev et al., 2016), showed behavioural, but no neural effects. Furthermore, we only have evidence of a single dissociation that shows a causal stimulation effect specific to value-based, and not perceptual choice. What candidate region would show a causal effect that is specific to perceptual, not value-based decisions in a way that would demonstrate a double dissociation?

Seminal human imaging studies have repeatedly implicated the superior frontal sulcus (SFS), a posterior portion of the dorsolateral prefrontal cortex (dlPFC), during perceptual decision-making (Heekeren et al., 2004, 2008; Mulder et al., 2014). While these studies have shown correlational evidence, it remains challenging to establish whether the SFS is directly involved in evidence accumulation or whether its observed activity reflects upstream or downstream support processes (e.g., attention or working-memory maintenance) rather than the accumulation computation per se**.** In this context, it is conceivable to imagine that the SFS would only play a role in a broader network that is not specific to the evidence accumulation process. Moreover, causal evidence from human studies

is difficult to obtain because most prior causal studies were only limited to one type of choice or performed in animals, and it is unclear if findings can be translated from animal models to human decision-making. However, disruption of human left SFS with non-invasive stimulation has been shown to impact behavioural performance and response speed in a dynamic face-house classification task, in a manner consistent with a reduction of evidence accumulation during decision-making. However, the domain-specificity of SFS contribution is unclear. Some studies have shown that dlPFC activity may reflect value-based evidence integration (Basten et al., 2010; Sokol-Hessner et al., 2012), suggesting the domain-generality of prefrontal function (Owen, 1997; Petrides, 2005). However, it is hard to directly compare the implicated neural processes to those that underlie perceptual decision-making processes, due to major differences in the stimuli and experimental approaches classically used in each domain (Gold and Shadlen, 2007; Heekeren et al., 2004), and that direct and principled comparisons with other decision-making domains, in general, are largely missing.

Here, we test the domain-specificity of the left SFS, and address the crucial double-dissociation gap in the literature by applying continuous theta-burst transcranial magnetic stimulation (cTBS) followed by functional magnetic resonance imaging (fMRI) while human participants alternated between matched perceptual and value-based choices (Polanía et al., 2014, 2015). We modelled the observed behavioural changes with the DDM, allowing us to causally associate the stimulated SFS region to specific underlying latent subprocesses of the unfolding decision (Mulder et al., 2014; Polania et al., 2015) as well as BOLD activation. Thus, this common evidence accumulation framework provides us with clear testable hypotheses regarding possible effect patterns across behavioural, computational, and neural levels.

RESULTS

The experiment. We recorded functional magnetic resonance imaging (fMRI) data from hungry, healthy participants ($n = 20$) performing perceptual- and value-based choice-tasks in alternation (**Methods** and **Fig. 1b**). For perceptual decisions, participants chose the larger food item, while for value-based decisions, participants chose the food item that they would preferably receive and consume by the end of the experiment. The stimuli and motor responses were identical for both tasks, as in previous experiments (Polanía et al., 2014, 2015). Choice pairings were predetermined based on participant's individual subjective perceptual- and value-based ratings of the food items, obtained just prior to the scanning session. Perceptual evidence was defined as the size difference (SD) between the food items, whereas value evidence was defined as the difference in value ratings (VD) between the choice alternatives (see **Methods** and **Fig. 1b**). A choice was classified as correct when it was consistent with the previously acquired ratings regarding size and preference respectively, i.e., when the larger-rated item was chosen for perceptual decisions or the higher-valued item was chosen for value-based decisions (Polanía et al., 2014, 2015). Our sample size is well within acceptable range, similar to that of previous TMS studies (Philiastides et al., 2011; Rahnev et al., 2016; Jackson et al., 2021; van der Plas et al., 2021; Murd et al., 2021).

Our experiment was divided into pre- and post-stimulation blocks. After participants had performed four pre-stimulation session-blocks inside the scanner, they received continuous theta burst stimulation (cTBS) (Huang et al., 2005; Di Lazzaro et al., 2005, 2008) over the left SFS (MNI coordinates, $x = -24, y = 24, z = 36$; Heekeren et al., 2004; Philiastides et al., 2011; Grueschow et al., 2018). Following this intervention, participants completed four post-stimulation fMRI blocks. By comparing the effects of stimulation on both types of behaviour and brain activity between post- and pre-stimulation blocks, we identify the role of SFS for either type of decision making. In particular, we examined whether the SFS is indeed selectively involved in perceptual decisions as previously suggested (Heekeren et al., 2004, 2006; Rahnev et al., 2016; Philiastides et al., 2011).

Our initial fMRI analyses were conducted at two levels. The first analysis aimed to broadly identify brain areas recruited for each choice task and those common to both. In this analysis, we assessed the average BOLD activity at the task level (perceptual versus value-based), irrespective of evidence accumulation. The second analysis focused on areas representing evidence accumulation specific to each type of choice. Here, we assessed how BOLD activity is modulated by trial-by-trial evidence strength. For this analysis, we used evidence strength from each choice task (perceptual or value-based) as a parametric modulator and regressed trial-by-trial evidence strength with BOLD (see **Methods**).

Study hypotheses. Previous studies have identified the causal mechanistic role of the SFS in evidence accumulation during perceptual decision-making (Heekeren et al., 2004, 2006; Rahnev et al., 2016), and its effect on stimulation may arise from one of either two channels. That is, one study reported that SFS disruption during a speeded perceptual categorisation task reduced accuracy and increased response times (Philiastides et al., 2011) and found associated decreases in drift rate, the DDM parameter describing the efficiency of sensory evidence integration. In contrast, another human brain stimulation study suggested that behavioural changes due to SFS disruption during a perceptual two-alternative-forced-choice (2AFC) task reflect decreased in the decision threshold, characterised by faster response speed but decreased choice precision. Simulations with the same DDM modelling framework (Rahnev et al., 2016) suggested that the decision threshold parameter could account for individual behavioural changes. Simultaneously acquired fMRI data suggested that SFS does not code the rate of integration but rather the necessary amount of evidence to be accumulated for the perceptual choice at hand (Rahnev et al., 2016).

To this end, we hypothesise that if SFS neurons indeed selectively accumulate perceptual evidence, we should find that their inhibition by cTBS leads to decreases in choice precision and increases in reaction times, a behavioural pattern that corresponds to a decrease in the DDM drift-rate parameter, and to concurrent increases in BOLD signals (caused by prolonged neural evidence accumulation; **Fig. 2a-c**). Critically, a different pattern can be expected when SFS neurons are involved in setting the criterion, i.e., determining the amount of evidence that needs to be accumulated for a perceptual choice to be taken. In this case, SFS inhibition should result in decreases in both choice precision and reaction times, a decrease in the DDM boundary parameter (Rahnev et al., 2016), and a reduction in associated neural activity due to the lower amount of evidence accumulated during the shorter response time (**Fig. 2d-f**). Here we directly test these two contrasting scenarios, by characterising the behavioural, neural, and neuro-computational consequences of cTBS to the left superior frontal sulcus (SFS). Crucially, we also investigate for both possible outcomes whether the functional contribution of the SFS during decision making is indeed specific for perceptual choices, by comparing the results between the two matched types of choices.

Behaviour: validity of task-relevant pre-requisites. Before scrutinising the role of the left SFS for either type of choice, we first behaviourally and neurally confirmed the validity of our task paradigm. To establish a fair comparison between perceptual (PDM) and value-based decision-making (VDM), we must necessarily show that we can distinctly identify the brain regions associated for each type of choice, and that behaviour is systematically a function of their respective evidence measures. Initial visual inspection shows that choice accuracy/consistency systematically increases (**Fig. 2a**) and RTs become faster (**Fig. 2b**) the larger the evidence difference, and this holds across tasks and stimulation conditions. All behavioural and fMRI analyses were performed on valid trials only (see Methods for inclusion criteria). Behavioural regressions confirmed that our task design allowed for a clear computational separation of both choice types: during perceptual decisions, participants relied exclusively on perceptual evidence, as reflected in both increased choice accuracy (main effect SD, $\beta = 0.560, p < 0.001$ and VD, $\beta = 0.023, p = 0.178$; **Fig. 1b**) and faster reaction times (RTs) with larger perceptual evidence, but not value-based evidence (main effect SD, $\beta = -0.057, p < 0.001$ and VD, $\beta = 0.002, p = 0.281$; **Fig. 1c**). Conversely, participants relied only on value evidence during VDM, as evident from both choice consistency (main effect VD, $\beta = 0.249, p < 0.001$ and SD, $\beta = 0.005, p =$

0.826; **Fig. 1b**) and RTs (main effect VD, $\beta = -0.016, p = 0.011$ and SD, $\beta = -0.003, p = 0.419$; **Fig. 1c**) irrespective of the items' size difference. Thus, our results replicate previous findings obtained with a similar paradigm (Polanía et al., 2014, 2015; Grueschow et al., 2015) showing that participants can use exclusively task-relevant evidence to make choices, and they confirm the suitability of our paradigm for directly comparing perceptual and value-based decisions with matched stimuli and motor responses. Across sessions, RTs tended to shorten in both tasks. In line with the HDDM results—selective boundary reductions for PDM and selective nDT shortening for VDM—we interpret the VDM RT speed-ups as reflecting more efficient non-decision (sensorimotor) components rather than changes in evidence accumulation. To illustrate baseline trends, we provide session-wise RT trajectories in the Supplement (see **Supplementary Fig. 11** for RT-by-session). For completeness, group-mean accuracies by task are provided descriptively in **Fig. 3a**; inferential tests focus on evidence-specific effects and TMS-induced changes within task.

fMRI: VDM and PDM distinctly recruit brain processes, while recruiting similar visual and motor processes. In line with the behavioural results that participants depended on different evidence for the two types of choices, initial fMRI analysis revealed that neural activations strongly differed between choice types, despite the fact that participants saw the same images and gave the same motor responses.

We performed two levels of fMRI analyses. The first analysis examined average BOLD activity at the task level, contrasting perceptual versus value-based decisions, irrespective of whether the differences were driven by evidence accumulation or other cognitive processes. This initial analysis aimed to broadly identify brain areas recruited for each choice task and those common to both. First, we found visual and motor areas were jointly activated for both types of choices ($p < 0.05$, FWE-corrected with cluster forming thresholds at $T(19) > 2.9$; **Supplementary Fig. 1a** and **Supplementary Table 1**). Second, PDM led to stronger recruitment of the posterior parietal cortex whereas VDM led to stronger activations of the medial prefrontal cortex and posterior cingulate cortex (**Supplementary Fig. 1b** and **Supplementary Table 2**), all in line with previous findings (Grueschow et al., 2015).

Notably, the left SFS does not yet appear in this contrast analysis. This is because this initial analysis did not include the parametric modulator for evidence accumulation. At this stage, we were evaluating whether the brain can flexibly recruit distinct brain regions based on task design, irrespective of whether these differences arise from variations in evidence accumulation or other cognitive processes. The second analysis assessed how BOLD activity is modulated by trial-by-trial evidence strength. Here, we identified a parametric modulator for evidence accumulation and regressed it on BOLD activity using a general linear model. This analysis revealed that the left SFS shows significant activation specifically when perceptual evidence is parametrically modulated. BOLD activity in the left SFS is detectable only when perceptual evidence is considered6. In fact, previous studies have similarly shown that the SFS only appears once a variable that measures the degree of evidence accumulation is included in the analysis6. Thus, these choice-type-specific brain activations, in response to identical visual input and motor output, ascertain that participants recruit task-specific brain regions depending on the choice domain.

Behaviour: theta-burst stimulation reduces choice accuracy for perceptual decisions only. Our results support the hypothesis that the SFS has a specific role for perceptual decision-making, on several experimental levels. Using a differences-in-differences (DID) logistic regression (**Methods**), we found that SFS-cTBS led to a significant decrease from pre- to post-cTBS blocks in accuracy for PDM (main stimulation effect, $\beta = -0.465 \pm 0.342, p = 0.008$; **Fig. 3a** and **Supplementary Fig. 2a**), while VDM choice consistency remained unaffected by SFS stimulation ($\beta = -0.042 \pm 0.205, p = 0.691$; **Fig. 3a** and **Supplementary Fig. 2a**). These differences were significant in direct comparison (stimulation × task interaction, $\beta = -0.094 \pm 0.087, p = 0.034$; **Fig. 3a**; **Supplementary Fig. 2c** and

Supplementary Table 2) fatigue or habituation effects after checking that the average accuracies in PDM were actually recovering in the second post-stimulation session while there was no change in choice consistency at all during VDM (**Supplementary Fig. 2a**). Interestingly, our DID linear regression (**Methods**) revealed that SFS-cTBS had comparable effects on reaction times in both tasks: faster RTs were observed after SFS-cTBS for both PDM (main stimulation effect, $\beta = -0.116 \pm 0.067, p = 0.003$; **Fig. 3b** and **Supplementary Fig. 2b**) and VDM (main stimulation effect, $\beta = -0.125 \pm 0.063, p = 0.001$; **Fig. 3b** and **Supplementary Fig. 2b**), with no significant difference between these two effects (stimulation × task interaction, $\beta = 0.009 \pm 0.069, p = 0.795$; **Fig. 3b**; **Supplementary Fig. 2c** and **Supplementary Table 2**). Overall, the specific changes in choice accuracy indeed reflect cTBS disruption in left SFS in perceptual decisions. At the same time, the common changes in RTs from the first to the second half of the experiment may not necessarily reflect TMS-related changes in SFS function but rather general training effects common to both tasks (Mawase et al., 2018), but this possibility can only be examined in more detail with computational modelling.

Modelling: SFS-TMS reduces decision boundary only for perceptual decisions. To examine in detail which specific latent decision process was affected by SFS-cTBS, we fit the hierarchical drift diffusion model (HDDM) simultaneously to the accuracy and RT data of our participants. This canonical model of choices allowed us to identify and disentangle the effect of stimulation on various latent variables representing distinct components of the choice mechanism (Ratcliff and Smith, 2004; Ratcliff and McKoon, 2008; Polania et al., 2015; **Supplementary Fig. 3** and see **Methods**).

To investigate the underlying processes through which the cTBS stimulation induced the observed behavioural changes, we fitted a hierarchical Bayesian drift-diffusion model (HDDM; see **Methods**) simultaneously to the accuracy and RT data of our participants (**Fig. 3b-d**). Critically, we used the DDM parameters to identify and disentangle the effect of stimulation on choice accuracy from that on RTs (Ratcliff and Smith, 2004; Ratcliff and McKoon, 2008; Polania et al., 2015; **Supplementary Fig. 3** and see **Methods**). A specific focus of this analysis was on whether SFS-cTBS would change the way participants set the choice criterion (decision threshold; Rahnev et al., 2016; Bogacz et al., 2010; Domenech and Dreher, 2010; Herz et al., 2016) or the efficiency with which choice-relevant evidence is accumulated (drift-rate, Philiastides et al., 2011; Basten et al., 2010) (see **Methods** for more details and **Fig. 1b,e**). We found that theta-burst stimulation selectively reduced the decision boundary in perceptual decision making (PDM) (see **Methods**; $p_{mcmc} = 0.003$; **Fig. 3c** and **Supplementary Fig. 5a**), while leaving the decision-relevant parameters, including the drift rate, unchanged ($p_{mcmc} = 0.822$ for drift rate; **Fig. 3d** and **Supplementary Fig. 5b,c**). For VDM, by contrast, no effect of cTBS was observed for either of the two decision-relevant parameters ($p_{mcmc} = 0.115$ for boundary and $p_{mcmc} = 0.758$ for drift rate; **Fig. 3c,d** and **Supplementary Fig. 5a,b,c**), supporting the specificity of the SFS involvement in perceptual decisions. Full posterior summaries are provided in **Supplementary Tables 8–11**, and model adequacy is confirmed by posterior-predictive checks of accuracies and RT distributions (**Supplementary Figs. 11–17**).However, we found that non-decision time (nDT) was selectively reduced in VDM**.** Overall, our findings indicate that the left SFS is causally involved in modulating the decision threshold. This conclusion was further corroborated by direct comparison of these effects, which showed that SFS-cTBS had a significantly stronger impact on the boundary parameter for PDM compared to VDM (stimulation × task interaction for the decision threshold, $p_{mcmc} = 0.045$; **Supplementary Fig. 5a**; there were no such differences for drift-rate; $p_{mcmc} = 0.685$; **Supplementary Fig. 5b**).

Modelling: faster RTs during value-based decisions is related to non-decision-related sensorimotor processes. To address the underlying latent process driving RT effects in both choices, we examined other DDM parameters and measurements. The DDM assumes that RTs can be disentangled into a non-decision-related (nDT) component as well as decision times (DT). The nDT is a DDM parameter that indexes constant latencies associated with sensory and motor preparation

processes that are invariant across trials with different choice evidence (Verdonck and Tuerlinckx, 2016; Starns and Ma, 2018); in other words, this parameter forms no part of the evidence accumulation process (Feltgen and Daunizeau, 2020; White et al., 2018) and may therefore reflect task learning processes from movement repetition (Mawase et al., 2018). In contrast, decision times is the component of RT where evidence accumulation actually takes place, and we can measure and derive DT using the evidence-dependent DDM parameters (see **Methods** for more details).

Our results showed that the faster RTs observed for value-based decisions after the stimulation indeed did not reflect evidence-dependent choice processes, but rather a change in non-decision-related sensorimotor processes (nDT) (see **Methods**; **Supplementary Fig. 3**): this parameter was decreased after stimulation for VDM ($p_{MCMC} = 0.062$) but not PDM ($p_{mcmc} = 0.707$) (**Supplementary Fig. 4b** and **5c**), with a significant difference between these effects ($p_{mcmc} = 0.041$; **Supplementary Fig. 5c**). In contrast, estimated decision times was smaller after stimulation during PDM ($p_{mcmc} = 0.003$; **Supplementary Fig. 6a**, left), but not VDM ($p_{mcmc} = 0.100$; **Supplementary Fig. 6a**, right). Taken together, these results suggest that the simultaneous change in RT reveal completely different computational processes, whereby faster RTs during value-based choice is simply a by-product of task-related learning that may perhaps be unrelated to stimulation, while faster RTs during perceptual choice is actually related to decision-relevant, evidence-dependent latent choice processes. However, completely ascertaining whether such effect from stimulation is due to SFS inhibition, we need clear causal evidence of changes from neural processing. The pattern of non-decision time and decision-time changes is consistent with the posterior-predictive fits shown in **Supplementary Figs. 11–17**, with numerical posterior summaries in **Supplementary Tables 8–11**.

fMRI: SFS activation changes for perceptual choices in line with model predictions. To investigate whether our behavioural and computational results directly relate to task-specific disruption of neural activity in left SFS, we investigated BOLD response changes in this brain area after stimulation. We exploited the fact that our fitted DDM and its latent parameters make clear predictions about how BOLD responses in this area should change if the stimulation affects the neural computations involved in setting the boundary for the necessary amount of evidence accumulation. Importantly, these predictions translate to clear parametric regressors that we can use for trialwise analysis of fMRI data (Basten et al., 2010; Domenech et al., 2017; Liu and Pleskac, 2011). More specifically, we expected that the BOLD signal level is proportional to the DDM's accumulated evidence (*aE*), defined as the area below the modelled evidence accumulation curve up until the accumulator reaches the decision boundary (Liu and Pleskac, 2011; Domenech et al., 2017; Basten et al., 2010). Using subject-wise DDM latent parameters, the average area below the decision boundary for each evidence level can be computed as a function of each participant's decision boundary divided by the mean drift rate (see **Fig. 1c** and **1f** and **Methods** for more details). Using the more detailed trialwise measures, however, the same area can be computed as a function of each trial's RTs divided by the evidence level, since according to the DDM, the duration of response times is directly proportional to the decision boundary, and the evidence level is directly proportional to the slope of the drift rate (Ratcliff and Rouder, 1998; Ratcliff and McKoon, 2008; see **Methods** for more details). Exploiting these two known facts from the DDM thus allows us to extend our test of the stimulation effect from individual-specific latent parameters to trialwise regressors and behavioural measures. Higher SFS BOLD signals are associated with higher aE and vice versa (Basten et al., 2010; Liu and Pleskac, 2011; Filimon et al, 2013; Tosoni et al., 2008), implying that a TMS intervention lowering the decision boundary should lower aE and therefore BOLD signals. Crucially, these latent changes predicted by the DDM should also be reflected in the subject-level simulations of accumulated evidence constructed from the DDM parameters.

Thus, we first tested whether our neural hypotheses would already be evident in the simulated trial-wise aE regressors. We used individual parameters identified by fitting our computational framework to simulate expected neural activity on a trial-wise basis across participants. To this end, we derived the predicted aE from the model parameters for each participant. A comparison across cTBS and task

conditions confirmed the predicted cTBS-related decrease in accumulated perceptual evidence for PDM ($p_{mcmc} = 0.003$; **Fig. 4a** and **Supplementary Fig. 6b**), the corresponding null effect for VDM ($p_{mcmc} = 0.100$; **Fig. 4b** and **Supplementary Fig. 6b**), and a significant difference for this effect between both choice types (one-sided $p_{mcmc} = 0.048$; **Supplementary Fig. 6b**).

In the next step, we used the trial-by-trial accumulated evidence as a regressor in the statistical analysis of the BOLD signals, allowing us to test whether the left SFS shows the predicted changes in neural response to varying levels of perceptual evidence. First, we tested whether our predictor of neural accumulated evidence was represented in BOLD signals of similar task-specific areas as reported previously for PDM in SFS (Heekeren et al., 2004, 2006) and for VDM in vmPFC (De Martino et al, 2013; Grueschow et al., 2015). This was confirmed by the data: During PDM, trialwise *aE* correlated with BOLD activity in the left SFS (peak at = −21, = 26, = 37; SV < 0.05; **Supplementary Fig. 7b** and **Supplementary Table 3**) whereas, critically, no significant BOLD activity in the left SFS was observed during VDM. During VDM, *aE* related to BOLD activity in the ventromedial prefrontal cortex (vmPFC) (peak at = 3, = 38, = −17; SV < 0.05; Supplementary Fig. 7e) and the nucleus accumbens (peak at *x* = 9, *y* = 11, *z* = −11; < 0.05, FWE-corrected with cluster-forming thresholds at $T(19) > 2.9$; Supplementary Fig. 7e). For both types of choices, domain-general representations of aE were also evident (see **Supplementary Fig. 7** and **Supplementary Table 3**).

We then tested whether cTBS specifically reduced the neural representation of accumulated perceptual evidence in the left SFS for PDM, as predicted by the behavioural and modeling results. In line with these predictions, comparison of the post − pre trial-aE regressor showed a lower BOLD response in left SFS to the trialwise perceptual evidence during PDM (SV < 0.05; **Fig. 4c**, green patch). This effect was significantly stronger than the corresponding effect on evidence representations in this area during VDM (SV < 0.05; **Fig. 4c**, blue patch). No effect was found for VDM alone. This indicates that the TMS effect is specific to the SFS during perceptual decisions, not value-based ones, as supported by the BOLD activity analysis**.** The reduction in BOLD activity in the left SFS during PDM after TMS is consistent with the DDM prediction of a reduction in the accumulated evidence due to a lower decision boundary**.** Convergent evidence for the specificity of this effect was provided by an alternative hypothesis-guided region-of-interest (ROI) analysis of the regression weights extracted from an a priori ROI-mask of the SFS (see **Methods**). This showed lower post-stimulation beta values for the trial-*aE* regressor during PDM (main stimulation effect, $\beta = -0.153 \pm 0.054, p = 0.004$; **Fig. 4a**) but not VDM (main stimulation effect, $\beta = 0.078 \pm 0.053, p = 0.140$; **Fig. 4b**) and a significant difference in these effects (stimulation × task interaction, $\beta = -0.232 \pm 0.075, p = 0.002$; **Fig. 4a,b**). Thus, the fMRI results show that cTBS of the left SFS indeed affects neural processing in this brain structure selectively during perceptual choices, in a way that is consistent with a lowering of the boundary and less accumulated evidence as predicted by the fitted DDM model. This remarkable convergence between the behavioural, modelling, and fMRI results suggests that the left SFS is indeed causally involved in setting decision criteria for choices based on perceptual evidence, but not based on subjective values.

fMRI and modelling: neural-HDDM shows that perceptual-choice accuracy and boundary setting reflect trial-by-trial changes in SFS activity. If perceptual-decision performance depends specifically on activity in the left SFS, then trial-wise choice accuracy should relate to trial-wise BOLD activity in the SFS during perceptual decisions, over and above the mean effects of evidence level. To test this, we regressed choice accuracy/consistency on trial-by-trial BOLD activity extracted from the left SFS ROI, choice type, and TMS, while controlling for the evidence provided by the stimulus pairs on each trial (see **Methods** for details). In line with our prediction, we observed that the relation between perceptual-choice accuracy and trial-by-trial SFS activity was significantly decreased by TMS (SFS × stimulation interaction, $\beta = -0.196 \pm 0.128, p = 0.003$; **Fig. 4d**), independently of the corresponding effects for choice evidence (SD main effect, $\beta = 0.524 \pm 0.082, p < 0.001$, VD main effect, $\beta = 0.197 \pm 0.012, p = 0.001$, SFS × SD interaction, $\beta = -0.041 \pm 0.046$, $p = 0.365$, SFS ×

VD interaction, $\beta = 0.055 \pm 0.041, p = 0.183$). This effect was clearly specific for PDM, since no such effects were observed for VDM (SFS × stimulation interaction $\beta = 0.099 \pm 0.242, p = 0.422$; SFS × stimulation × task interaction, $\beta = -0.072 \pm 0.051, p = 0.005$; **Fig. 4d**) and for RTs during both types of choices (SFS × stimulation interaction, perceptual: $\beta = -0.031 \pm 0.053, p = 0.367$; **Fig. 4d**; accuracy: SFS × stimulation interaction, $\beta = -0.012 \pm 0.050, p = 0.650$; **Fig 4d**).

We further investigated whether the relation between trialwise SFS activity and choice outcome indeed reflected an SFS role for perceptual boundary setting, as suggested by the DDM results presented above. To confirm this neurally, we set up several DDMs with trialwise SFS activity as an additional modulator for DDM parameters (on top of choice evidence; see **Methods** and Herz et al., 2016, 2017; Turner et al., 2015). More specifically, we tested several neural-DDMs in which trialwise SFS activity either modulated the decision threshold only (**Model 1**; **Supplementary Fig. 8a**), the drift rate only (**Model 2**; **Supplementary Fig. 8b**), or both parameters separately (**Model 3**; **Supplementary Fig. 8c**) or jointly (**Model 4**; **Supplementary Fig. 8d**). We compared these neural HDDMs to our baseline HDDM without neural inputs (see **Methods** for more details and **Supplementary Fig. 3**), allowing us to test across all conditions and choice types whether model evidence was enhanced when adding a potential trial-by-trial influences of SFS activity to the experimental inputs. Thus, the reported model evidence criterion (DIC) provides an additional formal test of whether the cTBS-influenced SFS activity relates selectively to the decrease of the decision boundary for perceptual choices only. Consistent with this prediction, Model 1 where SFS activity modulated the decision threshold only, outperformed all other models and model evidence showed improvements versus the baseline model (relative $DIC = -28.65$; **Fig. 4b**). These results provide direct evidence that neural computations in the left SFS support criterion setting for perceptual evidence accumulation.

fMRI and connectivity: TMS affects SFS functional connectivity during perceptual choices. Overall, our results clearly indicate that cTBS to the left SFS disrupts selectively a neural process related to setting the criterion for perceptual evidence accumulation. At this point, we consider the possibility that cTBS may conceivably change the functional communication of the SFS with other brain areas involved in initial processing of the perceptual information necessary to make a choice. We explored this possibility by investigating whether cTBS affected functional coupling of the SFS. A psychophysiological interaction (PPI) analysis seeded in left SFS and modulated by *aE* indeed revealed stronger coupling with occipital cortex (OCC) after cTBS (peak at $x = -28, y = -85, z = -2$; $p < 0.01$ FWE-cluster-forming thresholds at $T(19) > 2.9$; **Fig. 5a**). Interestingly, the activity peak in visual cortex showing evidence-dependent coupling with SFS, overlaps with the spatiotopic neural representation of the stimulus items in the visual field during decision making. We identified this overlap using a conjunction analysis of the PPI result and a contrast regressing BOLD signal on trial-by-trial stimulus onsets of both choice types (at familywise-error-corrected thresholds). Moreover, we used the latter contrast to define fully independent regions-of-interest (ROIs) in occipital cortex processing the visual stimuli independent of task type and performed an ROI analysis on the individual SFS-OCC-PPI betas extracted for each participant. This confirmed that evidence-related functional coupling is increased by stimulation during PDM (main stimulation effect, $\beta = 0.330 \pm 0.284, p = 0.022$) but not VDM (main stimulation effect, $\beta = -0.186 \pm 0.247, p = 0.139$; **Fig. 5b**; stimulation × task interaction, $\beta = 0.517 \pm 0.44, p = 0.021$; **Fig. 5a**). Thus, our exploratory analysis shows that cTBS to the left SFS leads to stronger functional coupling with occipital areas involved in processing the visual stimuli, perhaps consistent with increased downstream demand on visual-related resources when upstream evidence accumulation regions are impaired.

We further explored whether this TMS-induced increase in functional coupling between the left SFS and OCC is related to changes in behaviour and specific neural computations during perceptual decisions. To test this, we related these effects to individual measures of choice behaviour and latent DDM parameters for each participant. This revealed that stimulation-induced increases in SFS-OCC coupling were associated with lower accuracy (OCC × stimulation × task interaction, $\beta = -0.225 \pm$

$0.142, p = 0.002$; **Fig. 5c**) and shorter RTs (OCC × stimulation × task interaction, $\beta = -0.325 \pm 0.238, p = 0.007$; **Fig. 5c**) for PDM, but not VDM. Taken together, these results show that the causal behavioural and computational changes during perceptual decision-making due to left SFS-TMS may relate not just to local neural changes in SFS, but also to the way this brain structure communicates with visual cortex.

DISCUSSION

Our study shows that the left SFS serves a domain-specific causal role in the accumulation of perceptual evidence, and particularly, the underlying computations affected by non-invasive brain stimulation is the setting of the choice criterion during perceptual, but not value-based choice. Our findings are more in line with that of Rahnev et al. (2016), who also suggested that SFS disruption leads to lower threshold setting**.** In contrast, previous work has also shown that SFS activity correlates with the evidence accumulation process reflected by the drift rate. These findings are not necessarily incompatible, but rather, they may reflect the interlinked computational mechanisms of the SFS in perceptual evidence accumulation, where the SFS plays a role in setting the decision threshold. Furthermore, our findings, in a way, contribute in closing the double dissociation gap left by previous work (Polanía et al., 2015), where it was shown that frontoparietal connectivity is causally specific to the precision of value-based, not perceptual choice using the same matched perceptual- and value-based choice task. More importantly, our study provided results above and beyond current standards of causal studies in humans (Philiastides et al., 2011; Rahnev et al., 2016; Polanía et al., 2015; Murd et al., 2020), that was only observed in animal studies (Ding and Gold, 2012b; Erlich et al., 2015; Hanks et al., 2015). Here, we simultaneously showed that causal TMS effects affected behaviour, latent computations, and more crucially, neural circuitry, as observed by changes in fMRI-BOLD activation after stimulation.

Many human decision neuroscience studies have employed model-based approaches to identify BOLD signals that correspond to computational processes (Forstmann et al., 2011; Palmeri et al., 2017; Wijeakumar et al., 2017). However, the links between neural and latent computational processing established by these studies is largely correlational (Logothetis, 2008; Poldrack, 2006; Ramsey et al., 2010), and there are many model alternatives that could possibly account for BOLD signals. Our study illustrates that causal manipulations induced by targeted functional inhibition of brain areas can provide decisive information and provide more direct support for neurocomputational mechanisms posited by cognitive models. Specifically, our study underlines that the DDM provides a plausible mechanistic account of the decision process (Herz et al., 2016, 2017; Turner et al., 2015), by showing that left SFS inhibition by cTBS affects the evidence representation posited by the model consistently across behavioural, computational, neural, neural-behavioural levels. Importantly, our results directly link changes in behaviour to changes in both latent computations and neural processing, by demonstrating how raw trialwise neural signals from the left SFS can augment the DDM to explain behaviour. This suggests that once brain stimulation studies have established (causal) correspondence between neural activity and latent variables in decision models, such models can be fruitfully extended by neural measures to provide a more complete characterisation and prediction of choice behaviour and potentially its malfunctions. Our fMRI inferences rest on model-based assumptions linking accumulated evidence to BOLD amplitude. Alternative mechanisms—such as time-dependent (collapsing) boundaries—could attenuate the prediction that weaker-evidence trials yield longer accumulation and larger BOLD signals. While our behavioural and neural results converge under the DDM framework, we acknowledge this as a general limitation of model-based fMRI. The within-participant design enhances statistical sensitivity, yet the absence of an a priori power analysis constrains our ability to rule out small effects, particularly for null results in VDM.

Specificity of the SFS during perceptual decisions – only in humans? To this end, our study reinforces already established findings by showing that the causal role of SFS during perceptual decisions (Heekeren et al., 2004, 2006; Philiastides et al., 2011; Rahnev et al., 2016) is a specialised function of evidence integration. Furthermore, our finding of a selective role of left SFS in perceptual evidence accumulation is particularly intriguing. The area appears to be uniquely developed in the human brain, with no close anatomical homologue in other species. In the animal literature, most prefrontal disruption studies in non-human primates have focused on the frontal eye fields (FEF) (Ding and Gold, 2012a; Hanks and Summerfield, 2017; Shadlen and Newsome, 1996) and in rodents on the frontal orienting fields (FOF) (Erlich et al., 2015; Hanks et al., 2015). While we and others observed disruption of the evidence accumulation process after interfering with SFS function in humans (Philiastides et al., 2011; Rahnev et al., 2016), disruption of the FOF in rodents has not affected behaviour at all or in a qualitatively different manner (Brody and Hanks, 2016; Erlich et al., 2015; Hanks et al., 2015). However, the results of electrical stimulation of the FEF in monkeys (Ding and Gold, 2012a; Hanks and Summerfield, 2017) cannot necessarily be directly compared with TMS studies of human SFS, since FEF and SFS in humans are both structurally and functionally distinct (Murd et al., 2020; Rahnev et al., 2016). Thus, while it is tempting to speculate that the SFS perceptual evidence accumulation process identified here may be specific to humans, it is possible that researchers may have to further consider other putative homologues across species that may truly correspond to the SFS area stimulated here (Brunton et al., 2013; Hanks and Summerfield, 2017).

Do value-based decisions also rely on distinct PFC areas? At the same time, our findings do not rule out the possibility of SFS involvement during value-based choice, where it may perhaps have a secondary function (but one that does not involve evidence accumulation) or even other specialised functions in decision-making. For example, previous work has suggested that during value-based decisions, the dlPFC overall interacts with the vmPFC in modulating the value signal to facilitate self-control (Hare et al., 2009). Moreover, value-based decision-making entails a large array of choice types with varying degrees of complexity. For instance, more complex types of value-based decisions entail decisions under risk (Glickman et al., 2019), intertemporal choice (Peters and D'Esposito, 2020), and strategic and social decisions (Hutcherson et al., 2015), which may plausibly recruit the PFC due to working memory demands (Barbey et al., 2013), adjustment of decision time (Sokol-Hessner et al., 2012), or cost-benefit computations (Basten et al., 2010). In light of these many additional decision types based on preferences in the value-based choice domain, the functional specificity of SFS to perceptual decisions we claim here may have to be viewed with caution. Future studies should consider exploring the comparison between more complex types of value-based decisions with perceptual decisions, while taking great care in matching the degree of complexity between the two choice domains to avoid confounds induced by context or task difficulty.

The role of SFS in choice criterion setting during perceptual decisions. That being said, the same holds true with the varying degrees of complexity across perceptual decision-making processes. Our findings show that the mechanism of which the left SFS is causally involved is modulating the decision threshold, with clearly consistent results across behavioural, computational, neural, and neural-behavioural levels. Our findings are more in line with that of Rahnev et al. (2016), who also suggested that SFS disruption leads to lower threshold setting. In contrast, previous work has also shown that SFS activity correlates with the evidence strength in the accumulation process, as reflected by the drift rate (Basten et al., 2010; Heekeren et al., 2004, 2006). In support of this notion, cortical activity disruption with repetitive transcranial magnitude stimulation (rTMS) resulted in lower choice accuracy and slower RTs (Philiastides et al., 2011). However, it is important to note that these results are not at all incompatible, but reflect the interlinked computational mechanisms of the SFS in perceptual evidence accumulation. All these studies, including ours, point out that the DDM's drift rate and decision boundary are both decision-relevant latent mechanisms with distinct as well as overlapping implications on choice behaviour: impairments in both boundary and drift lead to lower choice consistency (Cavanagh et al., 2011; Green et al., 2012; Herz et al., 2016; Philiastides et al., 2011; Rahnev et al., 2016). The main difference in fact concerns reaction times: lower drift rate implies slower

RTs while a lower boundary implies faster RTs. The differences in RT-TMS effects of our study and that of Philiastides et al. (2011) may reveal the differences in task design and the nature of the stimuli. For instance, the study by Philiastides et al. (2016) used dynamic series of briefly presented sequential face-house stimuli, varying the strength of each stimulus within noise to vary the evidence levels. By contrast, our study and that by Rahnev et al. (2016) presented a static stimulus pair simultaneously during a 2AFC task and varied evidence not with noise but by stimulus difference.

We speculate that the goals of these tasks (i.e., discriminability from noisy dynamic stimuli versus stimulus size difference between static stimuli) may sensitively affect different latent processes. Previous studies have shown that different tasks can produce proximally similar behaviour but may involve different goal functions and therefore, computationally distinct processes (Heng et al., 2020). For instance, noisy dynamic stimuli entail the accumulation of sensory evidence until the decision-maker can form representations suitable for choice discrimination (Ratcliff and McKoon, 2008); thus, such stimuli are sensitively modulated by evidence strength, and reflected by a lower drift-rate when SFS is impaired (Philiastides et al., 2011) and where consequently, the circuitry takes more time to form perceptual representations. In contrast, evidence in the form of size difference may depend on the sensitivity to which SFS can detect the difference, and this is modulated by the decision threshold (Herz et al., 2016; Cavanagh et al., 2011; Green et al., 2012, 2013). Here, SFS impairment to accumulate evidence in the context of static, simultaneously presented stimuli may result in the inability of the circuitry to reliably discriminate size differences, resulting in the early termination of the accumulation process, which is behaviourally reflected as lower choice accuracy and faster RTs and computationally as lower thresholds. While a common evidence framework can plausibly reconcile our findings and that of previous studies, future studies should consider addressing this issue directly, by comparing the different goal functions and stimulus displays within perceptual decision-making tasks.

Functional coupling between left SFS and visual cortex. Furthermore, our study further expands our understanding of SFS function vis-à-vis other brain regions. It is well-established that the prefrontal cortex is structurally connected with many other brain regions (Wycoco et al., 2013) and may flexibly interact functionally with different areas depending on choice demands. Our exploratory connectivity results suggest that the SFS role for domain-specific accumulation of perceptual evidence is not just a local phenomenon but extends to functional communication with visual areas. Inhibition of this area's functional contribution to evidence accumulation led to an increase in its functional coupling with areas in occipital cortex representing the stimuli visually upon which choices were based. The changes in functional coupling strength between the two cortical regions also corresponded to observed behavioural and latent computational changes. This suggests that perceptual choices rely not only on local processing in SFS but on an integrated functional circuit, comprising both SFS and occipital cortex, at least for decisions based on visual stimuli as studied here. Though exploratory, our results are generally consistent with an occipito-frontal information exchange but extend it specifically to the SFS during perceptual evidence accumulation (Bullier et al., 1996).

We can speculate why the occipital cortex may have been recruited after inhibition of the left SFS via cTBS stimulation. For example, it is possible that cTBS-related impairments in the accumulation mechanism implemented by the SFS biases the system to rely on second-best suboptimal mechanisms for solving the tasks, such as template matching from working memory. Previous work has provided converging evidence that maintenance of visual information in working memory enhances coupling between sensory processing in visual cortex and information storage in lateral prefrontal cortex (Gazzaley et al., 2007; Serences et al., 2009). In fact, it has been suggested that SFS is canonically organised in "memory receptive fields" (Postle, 2016) that may be more heavily taxed when direct accumulation mechanisms for sensory input are impaired, as in the case of cTBS manipulations. Of course, there are many other candidate mechanisms, such as attention or working memory, that may be more heavily taxed to compensate for the excitability manipulation of the SFS area specialized for processing the sensory evidence, as suggested by previous work on prefrontal-occipital interactions during various attention and working memory tasks (Zanto et al., 2011). Overall,

the exploratory nature of our analysis warrants future investigation on the directionality of information flow between occipital cortex and SFS. Additionally, future studies should also test whether perceptual choices based on other sensory modalities (e.g., touch, audition) lead to a flexible coupling of SFS with the specific sensory areas processing these stimuli. In any case, our study shows clearly that in the healthy, undisrupted human brain, left SFS plays a key role in transforming perceptual evidence into choices.

Implications for theories of PFC organisation. Our study also contributes to our understanding of prefrontal cortex (PFC) functional organisation, given the considerable debates surrounding its organising principles (Owen, 1997). Previous studies have posited that different PFC regions contribute to specific aspects of information processing, in a manner that that can be flexibly applied to all types of information, be it from different sensory modalities or in different cognitive formats (Petrides, 2005). Prevailing perspectives have also proposed an anterior-to-posterior hierarchy in PFC for the purpose of general cognitive control and executive function (Nee and D'Esposito, 2016), suggesting that the main role of the PFC is largely in the domain of higher-order cognitive and abstract operations that transcend specific functional domains (Domenech and Koechlin, 2015; Koechlin and Summerfield, 2007). In contrast, our finding of a domain-specific causal role of SFS in evidence accumulation for perceptual decision-making suggests that the PFC is organised as a collection of fractionated sub-regions, such that each region processes different types of information (Goldman-Rakic and Leung, 2002), as opposed to a systematic hierarchy. Moreover, the fact that the SFS is even involved in the integration of low-level perceptual evidence (Heekeren et al., 2004, 2006, 2008; Philiastides et al., 2011; Rahnev et al., 2016) implies that the PFC's role is not limited to higher-order cognitive function. Overall, our findings are in no position of proposing an overarching framework of overall PFC organisation, given the limited area in posterior dlPFC targeted by our study, but rather a call to consider alternative views where the underlying organisational principles are more fractionated and less hierarchical.

Implications for computational psychiatry. Finally, our finding of SFS causal involvement in decision-threshold-setting during perceptual decision-making may offer clinical implications. Particularly, manifestations of impulsive behaviour (Heyes et al., 2012) are largely apparent in clinical populations with aberrations in decision threshold setting (Herz et al., 2016). However, most studies of these disorders have focused on impulsive behaviour induced by reward or preferences (Glimcher et al., 2007). It is important to note here that reward impulsivity is only one of the many domains of aberrant behaviour in clinical populations. Perceptual impulsivity is also important, since many of the behavioural and cognitive deficits are closely linked to impairments in perceptual function (Fuermaier et al., 2018). For instance, impulsive behaviour can also arise in non-reward-related settings, such as when perceptually discriminating size differences where less accurate and faster responses have been observed in people with addiction disorders (Banca et al., 2016) and borderline personality disorder (Berlin and Rolls, 2004). Perceptual deficiencies are also prevalent in clinical populations with attention-deficit hyperactivity disorder (ADHD) or Parkinson's disease, and thought to be linked to impairments in the dopaminergic system (Fuermaier et al., 2018). Prior causal evidence from deep-brain stimulation (DBS), in particular, has shown that disrupting the STN lowered decision thresholds, thus increasing this perceptual impulsivity among Parkinson's patients (Herz et al., 2016, 2017). Our findings that TMS of the left SFS causally and selectively lowered the decision boundary during perceptual decisions suggest that the lateral prefrontal cortex may be functionally integrated with these cortico-striatal and cortico-subthalamic nuclei (STN) pathways (Bogacz et al., 2010; Green et al., 2012, 2013).

Overall, impulsive behaviour is not exclusive to the reward domain, and our results suggest that there is something to gain from understanding impulsive behaviour in non-reward settings requiring decisions on perceptual information. Maladaptive behaviour may not only reflect individual wants or likings, often assumed by addiction studies, but could also be a function of low-level sensory or higher-order cognitive processes that have so far not fully been accounted for (Fuermaier et al., 2018). This

may have serious implications for how cognitive therapies or interventions are designed, and our findings may provide useful insights in guiding such future work. Particularly, it is worth exploring to what degree the left SFS and its connections are structurally or functionally different in clinical populations, and whether these impulsive tendencies can be captured by sequential sampling models, such as the DDM.

MATERIALS AND METHODS

Participants. Twenty healthy right-handed volunteers (ages 20-30; 8 female) with normal or corrected-to-normal vision participated in the study. Participants were fully informed about the features of the experiment. No participant suffered from any neurological or psychological disorder or took medication that interfered with their participation in the study. Participants received monetary compensation for participation and performance of the perceptual choices, as well as one food item to consume after the experiment depending on a random value-based choice trial. The experiments conformed to the Declaration of Helsinki and the experimental protocol was approved by the Ethics Committee of the Canton of Zurich.

Experimental paradigm. We asked participants to refrain from eating for 3 hours before the start of the experiment. Our experiments took place between 0800 and 1900 hr during the day. The experiment consisted of two steps: (1) a rating task outside the scanner and (2) a decision-making task inside the scanner. During the rating task, we asked participants to provide perceptual- and value-based ratings of the same set of 61 food images using an on-screen slider scale. All of the food items were in stock in our lab and participants were informed about this via visual inspection. For perceptual ratings, participants rated—on a scale from 5 to 100 percent in steps of 5 percent— how much of the black background within the white square perimeter was occupied by the food item. For value-based ratings, participants rated—on a scale from 5 to 100 in steps of 5—how much they wanted to eat the presented food item at the end of the experiment. We instructed participants that the midpoint of the scale in value-based ratings indicated indifference.

After rating the food items, an algorithm selected a balanced set of perceptual and value-based trials divided into four evidence levels, E. The evidence levels are based on the absolute difference between the average ratings of the food items paired in each trial. We define perceptual evidence as the absolute size difference between the two food items. On the other hand, we define value-based evidence as the absolute value difference between the two food items. In particular, the evidence levels for perceptual trials, E_p, are:

$$E_p = \left|r_{\mathbf{biggest}} - r_{\mathbf{smallest}}\right| \in \{5\%, 10\%, 15\%, 20\%\}$$

while the evidence levels for value-based trials, E_v, are:

$$E_v = \left|r_{\mathbf{best}} - r_{\mathbf{worst}}\right| \in \{1,2,3,4\}$$

where $r = \frac{r_1+r_2}{2}$ is the average food item from the two ratings while $r_{\mathbf{biggest}} - r_{\mathbf{smallest}}$ and $r_{\mathbf{best}} - r_{\mathbf{worst}}$ represent the ratings' difference for the pairs presented for perceptual and value-based choices, respectively.

Inside the scanner, participants performed the decision-making task for which they chose between two food items, based on whether they were accumulating perceptual or value-based evidence. We matched the visual sensory stimuli of the food items as well as their motor outputs across the two

choice types. The only difference was the type of evidence participants had to accumulate to make a choice. Each trial started with presentation of a central fixation marker (length ~ 0.8°, height ~ 0.3°). Next, a centrally presented word indicated whether participants would perform a perceptual (word 'AREA') or value-based (word 'LIKE') choice. On the subsequent screen, the task cue was replaced by either the letter 'A' or 'L' (~ 0.2°) to remind participants that they were in a perceptual or value-based block, respectively. Two food items were simultaneously displayed, one above and one below the screen (y eccentricity 3.6°; a white square of 6° width surrounded each food item). Blocks alternated between perceptual and value-based choices in a given session (7-9 trials per task block). Participants pressed one of two buttons on a keypad with their right middle finger (upper item) or right index finger (lower item) to indicate their choice. On a given trial, participants had 3 seconds for their choice; otherwise, the trial would be regarded as a 'missed trial' and would not enter the analysis. Analyses were conducted on valid trials only, defined as trials with a registered response within the task's response window and passing pre-specified validity checks; trials without a response were excluded and not analysed. Participants made correct or consistent choices when they chose the food item with the higher rating as indicated in the double ratings task prior to entering the scanner. After the experiment, participants stayed in the room with the experimenter while they ate the food that was selected based on the participants choice in one randomly selected VDM trial. During perceptual decisions-making blocks, participants were rewarded with 0.5 CHF every time they correctly discriminated between the size difference of the two food items presented on the monitor screen.

The experiment had a total of 256 trials divided into 8 sessions of 32 trials each. The first 4 sessions were pre-stimulation sessions where participants performed the task without stimulation. The last 4 sessions were post-stimulation sessions during which participants performed the choices with decreased neural excitability in the SFS due to the preceding continuous theta-burst stimulation. The 256 trials were fully balanced across all factors (trial type: perceptual or value-based; evidence levels: 1 to 4; correct response: up or down).

Stimulation protocol. We applied continuous theta-burst stimulation (cTBS) (Huang et al., 2005; di Lazzaro et al., 2005, 2008) to exogenously induce cortical inhibition of our region of interest (ROI), an area in the left superior frontal sulcus (SFS) (MNI coordinates: $x = -24, y = 24, z = 36$) (Heekeren et al., 2004; Philiastides et al., 2011). Before the main fMRI experiment, we identified the stimulation site over the left SFS (MNI coordinates: $x = -24$, $y = 24$, $z = 36$) (Heekeren et al., 2004; Philiastides et al., 2011) based on previous studies and each individual's stimulation intensity. In an initial fMRI session, we acquired high-resolution T1-weighted 3D fast-field echo anatomical scans used for subsequent neuro-navigation (181 sagittal slices, matrix size = 256 × 256, voxel size = 1 mm3, TR/TE/TI = 8.3/2.26/181 ms, 3T Philips Achieva). The hand area of the left M1 (motor hotspot) was determined by identifying the first dorsal interosseous (FDI) movement-evoked potentials (MEPs) induced by transcranial magnetic stimulation (TMS) pulses. We delivered single monophasic TMS pulses using a figure-of-eight coil attached to the TMS stimulator. We then marked an equidistant circular grid on each individual's anatomical MRI scan using a neuro-navigation system over the hand motor region, located at the anterior portion of the central sulcus. We localised the optimal motor hotspot as the point in the grid that elicited the strongest FDI MEPs from TMS pulses. Once we selected the motor hotspot, we asked participants to activate their FDI by pressing their thumb and index finger at about 20% maximum force in order to obtain their active motor threshold (AMT). We defined the AMT as the minimal TMS intensity required to produce MEPs of ≥ 200 mV amplitude (measured with Magventure MRi-B91) in ≥ 5–10 consecutive pulses. We retested the AMT by visually inspecting the FDI twitches triggered by TMS pulses over the marked optimal hotspot. The average AMT outside the scanner was 52.35 ± 6.27 percent while the AMT inside the scanner was 52.91 ± 6.18 percent. We applied cTBS at an intensity of 80% of the individual's AMT. The cTBS protocol contained bursts of 3 pulses at 50 Hz. This protocol has been shown to reduce cortical excitability for at least 30 minutes (Huang et al., 2005). Every burst was repeated at a rate of 5 Hz, resulting in 200 bursts with a total of 600 pulses delivered within 40 seconds.

Before moving our participant into the scanner, we marked the motor hotspot as well as the stimulation site on a swimming cap fixed in position by straps. Participants wore this cap while they were inside the scanner. Before the start of the fifth session, participants received cTBS over the left SFS. We used a figure-of-eight MR-compatible TMS coil (MRi-B91) attached to a TMS stimulator. Participants returned to the scanner after receiving stimulation and proceeded to complete the last four sessions. On average, the post-TMS fMRI task started 228 $\pm$ 41 sec after the end of theta-burst stimulation following established protocols from previous studies (Knecht et al., 2003; Philiastides et al., 2011; Thut and Pascual-Leone, 2010). Given the established timeline of cTBS effects (Huang et al., 2005), we expected the stimulation effects to weaken over time due to neural recovery. In line with established procedures, we treated the first two post-stimulation sessions as the actual post-cTBS period and the last two post-stimulation sessions as a recovery period (Philiastides et al., 2011).

Differences-in-differences. We implemented a differences-in-differences (DID) regression analysis to identify the causal relationships based on stimulation-induced neural inhibition in SFS. We used the identical DID for behavioural, computational, neuroimaging and connectivity analyses. Here, we use the following notation: task conditions $Task$ (perceptual, $Task = 1$; value-based, $Task = 0$); stimulation conditions TMS (pre- $TMS = 0$ and post- $TMS = 1$); V is our variable of interest, which may be behavioural or neural; and, the causal treatment effect, $\boldsymbol{\phi}(V|Task, TMS)$, takes the following form:

$$\begin{aligned}\boldsymbol{\phi}(V|Task, TMS) \\ &= [\mathbb{E}(V|TMS = 1, Task = 1) - \mathbb{E}(V|TMS = 0, Task = 1)] \\ &- [\mathbb{E}(V|TMS = 1, Task = 0) - \mathbb{E}(V|TMS = 0, Task = 0)]\end{aligned}$$

where $\mathbb{E}(V|Task, TMS)$ is the expected value of the variable of interest, V, given task and TMS condition. The first difference on the right-hand side captures the average stimulation effect for PDM while the second difference captures the average stimulation effect for VDM. The overall difference assumes that if behaviour will be the same after stimulation, then there is no effect, $\phi = 0$ (Angrist and Pischke, 2009; Bertrand et al., 2004). But if there is a stimulation effect and it impairs behaviour or neural activity, then $\phi < 0$.

Behavioural analyses for choice. We analysed the influence of continuous theta-burst stimulation on choice using a logit regression on choices, ρ (correct = 1, incorrect = 0) over various regressors of interest, such as TMS condition, TMS (pre-cTBS = 0, post-cTBS = 1); task, $Task$ (perceptual = 1, value-based = 0); its interaction ($Task \times TMS$), which measures the causal stimulation effect, $\boldsymbol{\phi}$; and, other regressors, X^k that we use as controls. This includes task-relevant evidence (SD for perceptual and VD for value-based, 1 to 4), response times (RTs), and task-irrelevant evidence (i.e. VD for perceptual and SD for value-based, 1 to 4). The full model is,

$$\Pr\left(\rho_{t,c,s,i}^{DID}\right) = \frac{1}{1 + \exp\left(-[\beta_0 + \beta_1 Task_{(t,c,s,i)} + \beta_2 TMS_{(t,c,s,i)} + \boldsymbol{\phi} Task_{(t,c,s,i)} TMS_{(t,c,s,i)} + \sum_{k=4}^{n} \beta_k X_{(t,c,s,i)}^k\right)}$$

where *t* indexes task, *c* for TMS, *s* for subject, and *i* for trial. Since our model contains a DID interaction term, nonlinearity of the logit regression results is a non-zero estimate even if the true causal effect is zero, $\phi = 0$.

To remove nonlinearity bias and isolate the true causal effect, we ran another logit regression without the interaction term,

$$\Pr\left(\rho_{t,c,s,i}^{NODID}\right) = \frac{1}{1 + \exp\left(-\left[\beta_0 + \beta_1 Task_{(t,c,s,i)} + \beta_2 TMS_{(t,c,s,i)} + \sum_{k=4}^{n} \beta_k X_{(t,c,s,i)}^k\right]\right)}$$

and we take the difference between the two logits (Ai and Norton, 2003; Karaca-Mandic et al., 2012; Puhani, 2012),

$$\Pr\left(\rho_{(t,c,s,i)}^{TRUEDID}\right) = \Pr\left(\rho_{(t,c,s,i)}^{DID}\right) - \Pr\left(\rho_{(t,c,s,i)}^{NODID}\right).$$

We also ran variations of the model to test for robustness, particularly GLMs with or without control variables, and we also tested robustness using various stimulation runs (see **Supplementary Table 5**). We used cluster-robust standard errors at the subject level under the assumption that each individual performance is independent across participants. We implemented this analysis using STATA/SE 13.1.

Behavioural analyses for response times. We similarly used DID regressions to analyse the influence of cTBS on response times (rt). Here, we simply ran a general linear model (GLM) for our regression,

$$rt_{t,c,s,i} = \beta_0 + \beta_1 Task_{(t,c,s,i)} + \beta_2 TMS_{(t,c,s,i)} + \boldsymbol{\phi} Task_{(t,c,s,i)} TMS_{(t,c,s,i)} + \sum_{k=4}^{n} \beta_k X_{(t,c,s,i)}^{k} + \varepsilon_{(t,c,s,i)}$$

and we also ran variations of the model (see also **Supplementary Table 5**). We similarly used cluster-robust standard errors at the subject level.

Hierarchical Bayesian DDM. We analysed the effect of cTBS on PDM and VDM using hierarchical drift diffusion model (HDDM). The model assumes a evidence is accumulated through a one-dimensional Wiener process, whereby the state of evidence, x_t at time t evolves through a stochastic differential equation,

$$\frac{dx_t}{dt} \sim \mathbb{N}(\delta, \sigma^2).$$

Here, δ is the amount of evidence being accumulated at time *t*,

$$\delta = \kappa_{c,s} E_{c,s,i}$$

where E represents the evidence level and κ is the drift-rate that linearly scales the evidence and this is typically interpreted as quality of information processing. The model assumes evidence is accumulated at the starting point, β, and the accumulation process continues until a choice, ρ, is made at time t_d at a given threshold, α. Once the accumulation process terminates, the state of evidence is either $x_t > \alpha$ (a correct decision) or $x_t \leq 0$ (an incorrect decision). We also accounted for visual sensory processing and motor response delays with the non-decision time parameter (*nDT*), τ.

The hierarchical Bayesian model is implemented whereby each observed choice, $y_{c,s,i}(\rho, rt)$, follows a Wiener distribution, ω,

$$y_{(c,s,i)} \sim \omega(\delta, \alpha, \tau, \beta)$$

where c indexes task ($c = p$ for perceptual, $c = v$ for value-based), s for participants ($s = 1, \ldots, N_{subjects}$), and i for trials ($i = 1, \ldots, N_{trials}$). Furthermore, the hierarchical structure contains three random variations at the trial, subject, and condition levels. We treated all interindividual differences per stimulation condition level as random effects:

$$\delta_{(c,s,i)} \sim N\left(\mu_{\delta(s)} E_{(c,s,i)}, \sigma^2_{\delta(s)}\right)$$

$$\tau_{(c,s,i)} \sim N\left(\mu_{\tau(s)}, \sigma^2_{\tau(s)}\right)$$

$$\alpha_{(c,s,i)} \sim N\left(\mu_{\alpha(s)}, \sigma^2_{\alpha(s)}\right)$$

where $N(\mu, \sigma)$ is a normal distribution with mean, μ and standard deviation, σ. Here, E represents the trial-by-trial evidence levels, which we measure in absolute terms; and we fix the starting point, $\beta_{c,s,i} =$ 0.5. We used Bayesian hypothesis testing to compare posterior probability densities.

Measure of accumulated evidence. We computed estimates for decision times ($t_{d(c,s)}$) and accumulated evidence ($aE_{c,s}$) to test whether aE is a plausible representation of the accumulation process at the neural level. Following the literature (Bogacz et al., 2006, 2010), we define mean decision time as the ratio between the decision threshold and the drift rate shaped by a hyperbolic tangent function,

$$t_{d(c,s)} = \left(\frac{\alpha_{c,s}}{\kappa_{c,s}}\right) \tanh\left(\kappa_{c,s} \times \alpha_{c,s}\right)$$

It is important to note that reaction time, rt, is the sum of both decision and non-decision times, $rt = t_d + \tau$.

We define accumulated evidence (aE) as the area below the drift process up until the accumulator reaches the decision boundary:

$$aE_{c,s} = \frac{\alpha_{c,s} \times t_{d(c,s)}}{2}.$$

Here, we derive aE using the area equation of a triangle, where decision time $t_{d(c,s)}$ is the base and the decision boundary, $\alpha_{c,s}$, is the height.

MCMC sampling. To estimate all parameters, we performed Gibbs sampling via Markov Chain Montecarlo (MCMC) in JAGS (Plummer, 2016) to generate parameter posterior inferences. We drew a total of 100,000 samples from an initial burn-in step and subsequently drew a total of new 100,000 samples with three chains each. We derived each chain based on different random number generator engines with different seeds. We applied a thinning of 100 to this final sample, resulting in a final set of 1,000 samples for each parameter. This thinning assured auto-decorrelation for all latent variables of interest. We conducted Gelman-Rubin tests for each parameter to confirm chain convergence. All latent parameters in our Bayesian model had $\hat{R} < 1.05$, suggesting that all three chains converged to a target posterior distribution. We compared the difference in posterior population distributions estimated for each parameter between the stimulation conditions as well as the differences-in-differences (DID), which included differences between tasks. We tested whether the resulting distribution (i.e., the causal stimulation effect) is significantly different from zero (i.e., the null hypothesis) using the cumulative function up to or from 0 depending on the direction of the effect. We refer to this probability as Bayesian "p-values," p_{mcmc}.

fMRI data analysis. Participants performed eight choice-task sessions while BOLD images were recorded with a Philips Achieva 3T whole-body scanner. We used statistical parametric mapping (SPM8, Wellcome Trust Center for Neuroimaging) for image pre-processing and analysis. In particular, images were slice-time corrected (to the acquisition time of the middle slice) and realigned to account

for subject's head motion. Each participant's T1-weighted structural image was co-registered with the mean functional image and normalised to the standard T1 MNI template using the new-segment procedure in SPM8. The functional images were normalised to the standard MNI template using the same transformation, spatially resampled to 3mm isotropic voxels, and smoothed using a Gaussian kernel (FWHM, 8mm).

We estimated two general linear models (GLMs), constructed by convolving a series of appropriately placed indicator functions with the default model of the BOLD response embedded in SPM8. GLM1 contained only two indicator functions for the onsets of PDM or VDM trials. On the other hand, GLM2 contained four indicator functions for the onsets of task (PDM and VDM trials) and stimulation (pre- or post-TMS) runs, coupled with one regressor each for parametric modulation of the BOLD response by the trialwise accumulated evidence (aE). We earlier demonstrated that the theoretical average accumulated evidence is derived from population-level as well as subject-level latent DDM parameters, by dividing the estimated decision boundary by the estimated drift rate. To construct a trialwise measure of aE, we exploit the fact that the length of the RTs is directly proportional to the size of the decision boundary while the evidence level, E, is directly proportional to the drift rate (Basten et al., 2010; Domenech et al., 2017; Kiani et al., 2014). With this mapping, we can then construct a parametric trialwise measure of accumulated evidence, $aE_{t,c,s,i}$,

$$aE_{t,c,s,i} = \sqrt{\frac{RT_{t,c,s,i}}{E_{t,c,s,i}}},$$

where the square root function accounts for the concave nonlinearity in accumulated evidence. Previous work (Tajima et al., 2016) has shown theoretically that the shape of the accumulated evidence is indeed concave, where it suggests that the rate of accumulating evidence is decreasing as the decision process continues to accumulate. This concavity in *aE* is consistent with DDM predictions where evidence accumulation is steeper during earlier responses and begins to plateau at later responses (Ratcliff and McKoon, 2008; Ratcliff and Smith, 2004).

We convolved our GLMs with a canonical haemodynamic response function (HRF), modelled MR image autocorrelations with first-order autoregressive model, and included 6 motion parameters (obtained during realignment) as regressors of no interest. After fitting the model to the BOLD data, we tested regressors for statistical significance at the second-level, in random-effects group one-sample t-tests of the corresponding single-subject contrast images. We performed statistical inference at the cluster level, using whole-brain family-wise-error-corrected (FWE-corrected) statistical threshold of $p < 0.05$, based on a cluster-forming voxel cutoff at $p < 0.005$ (or $T(19) = 2.9$). For hypothesis-guided region-of-interest (ROI) analysis (i.e., left SFS stimulation site, MNI coordinates: $x = -24, y = 24, z = 36$), we corrected for multiple comparisons using small-volume correction (SVC, $p < 0.05$) restricted within a 10 mm sphere around the target coordinates. We extracted neural betas from this spherical SFS ROI for each participant to perform hypothesis testing and correlational analysis.

Functional connectivity. We ran a psychophysiological interaction (PPI) analysis (Friston et al., 1997) to investigate the changes in functional connectivity between the left SFS and other brain regions due to cTBS. Here, we extracted physiological time series in the SFS seed region, which corresponds to the time-course of the first eigenvariate across all voxels in the region using principal component analysis (Friston et al., 1993). The psychological regressor corresponded to the difference in accumulated evidence, aE (as described in GLM2) between PDM and VDM. We generated PPI estimates from the psychological regressors and the time series from the left SFS, and we then computed the PPI contrasts-of-interest for PDM and VDM. Statistical inference on subject-specific PPI maps was performed using second-level random-effects analysis across participants to allow for group-level inferences. For each participant, we also extracted PPI neural betas, which measures the

degree of functional coupling between the left SFS, and we then performed hypothesis testing and correlational analysis.

Hierarchical Bayesian neural-DDM. We also analysed whether the inclusion of raw trial-by-trial BOLD response extracted from left SFS and attach it to any of the DDM parameters can improve model evidence. Such a result would suggest that neural activity in the left SFS directly related to the model's latent decision-relevant parameters. We used z-scored single-trial neural beta estimates extracted from the left SFS target site. We implemented four a-priori models regarding the role of the left SFS on the decision parameters: **Model 1** assumes that the left SFS modulated the decision threshold (**Supplementary Fig. 8a**), while **Model 2** assumes that left SFS modulated the drift rate (**Supplementary Fig. 8b**):

$$\alpha_{c,s,i}^{NEURAL} = \alpha_{c,s,i} + \gamma\theta_{c,s,i}$$

$$\delta_{c,s,i}^{NEURAL} = \kappa E_{c,s,i} + \gamma\theta_{c,s,i}$$

where γ is the scale parameter for trial-by-trial left SFS activity, θ. On the other hand, Models 3 and 4 assume that the left SFS modulates both boundary and drift: **Model 3** assumes separate scale parameters for each latent process (see **Supplementary Fig. 8c**) while **Model 4** assumes a common scale parameter for both boundary and drift (see **Supplementary Fig. 8d**). Model comparison used the Deviance Information Criterion (DIC = $\bar{D}$ + pD), where pD is the effective number of parameters; thus DIC penalizes model complexity, and lower DIC denotes better predictive accuracy after accounting for complexity. We then used the best model to re-estimate our latent parameters and to perform Bayesian post-hoc inferences.

Correlating causal changes between neural, latent, and behavioural variables. We tested whether there were any correlational changes between neural, v, and behavioural, π, measures after stimulation. The marginal effect, r, measures the correlational change in neural measure, ν, given behavioural measure, π,

$$r(\nu_{c,s}|\pi_{c,s}) = \frac{\partial}{\partial\pi_{c,s}}\mathbb{E}(\nu_{c,s}|\pi_{c,s}).$$

We test the marginal effect, r, of the correlational change between our neural and behavioural measures using our DID regression at trial and subject levels. With trialwise data, we used logit regression to test whether the marginal effect of trialwise changes in left SFS, $Neur$, will affect choices, ρ. Similar to previous models, we included various regressors of interest, especially the triple interaction ($Neur \times Task \times TMS$), which accounts for the causal TMS effect, $\boldsymbol{\phi}$, as well as other regressors, X^k. The full model is,

$$\begin{aligned}\Pr\left(\rho_{(t,c,s,i)}^{DID}\right) = \Bigg(1 \\ + \exp\Bigg[-\Bigg(\beta_0 + \beta_1 Task_{(t,c,s,i)} + \beta_2 TMS_{(t,c,s,i)} + \beta_3 Neur_{(t,c,s,i)} + \beta_4\left[Task_{(t,c,s,i)}TMS_{(t,c,s,i)}\right] \\ + \beta_5\left[Neur_{(t,c,s,i)}Task_{(t,c,s,i)}\right] + \beta_6\left[Neur_{(t,c,s,i)}TMS_{(t,c,s,i)}\right] \\ + \boldsymbol{\phi}\left[Neur_{(t,c,s,i)}Task_{(t,c,s,i)}TMS_{(t,c,s,i)}\right] + \sum_{k=4}^{n}\beta_k X_{(t,c,s,i)}^k\Bigg)\Bigg]\Bigg)^{-1}.\end{aligned}$$

To remove nonlinearity bias and isolate the true causal effect, we ran another logit regression without ϕ,

$$\Pr\left(\rho_{(t,c,s,i)}^{NODID}\right) = \Bigg(1 + \exp\Bigg[-\Bigg(\beta_0 + \beta_1 Task_{(t,c,s,i)} + \beta_2 TMS_{(t,c,s,i)} + \beta_3 Neur_{(t,c,s,i)} + \beta_4\left[Task_{(t,c,s,i)} TMS_{(t,c,s,i)}\right] + \beta_5\left[Neur_{(t,c,s,i)} Task_{(t,c,s,i)}\right] + \beta_6\left[Neur_{(t,c,s,i)} TMS_{(t,c,s,i)}\right] + \sum_{k=4}^{n} \beta_k X_{(t,c,s,i)}^{k}\Bigg)\Bigg]\Bigg)^{-1},$$

and then we took the difference between the two logit models,

$$\Pr\left(\rho_{(t,c,s,i)}^{TRUEDID}\right) = \Pr\left(\rho_{(t,c,s,i)}^{DID}\right) - \Pr\left(\rho_{(t,c,s,i)}^{NODID}\right).$$

We similarly ran a DID-GLM to test whether the marginal effect of trialwise left SFS neural betas will causally affect RTs,

$$\begin{aligned} rt_{(t,c,s,i)} = \beta_0 &+ \beta_1 Task_{(t,c,s,i)} + \beta_2 TMS_{(t,c,s,i)} + \beta_3 Neur_{(t,c,s,i)} + \beta_4\left[Task_{(t,c,s,i)} TMS_{(t,c,s,i)}\right] \\ &+ \beta_5\left[Neur_{(t,c,s,i)} Task_{(t,c,s,i)}\right] + \beta_6\left[Neur_{(t,c,s,i)} TMS_{(t,c,s,i)}\right] \\ &+ \boldsymbol{\phi}\left[Neur_{(t,c,s,i)} Task_{(t,c,s,i)} TMS_{(t,c,s,i)}\right] + \varepsilon_{(t,c,s,i)}. \end{aligned}$$

We also used cluster-robust standard errors at the subject level in all of our analysis.

With subject-level data, we similarly used linear mixed-effects regression models to test whether the marginal effect of subject-level neural betas (left SFS or PPI) ν, will affect behavioural outcomes or DDM-latent parameters, π. Similarly, we estimated the marginal effect, $\boldsymbol{\phi}$, with a three-way interaction, $(\nu \times Task \times TMS)$,

$$\begin{aligned} \pi_{(c,s)} = \beta_0 &+ \beta_1 Task_{(c,s)} + \beta_2 TMS_{(c,s)} + \beta_3 \nu_{(c,s)} + \beta_4\left[Task_{(c,s)} \times TMS\right] + \beta_5\left[\nu_{(c,s)} \times Task_{(c,s)}\right] \\ &+ \beta_6\left[\nu_{(c,s)} \times TMS_{(c,s)}\right] + \boldsymbol{\phi}\left[\nu_{(c,s)} \times Task_{(c,s)} \times TMS_{(c,s)}\right] + \varepsilon_{(c,s)}. \end{aligned}$$

This three-way interaction measures whether the correlations between neural activity (left SFS, PPI betas) and behaviour (choice, DDM parameters) are causally affected by stimulation, TMS, and whether the effect is specific only during the perceptual task.

DATA AND CODE AVAILABILITY

Behavioural and neuroimaging data and the code for data analysis are available at 10.17605/OSF.IO/3DMH9.

ACKNOWLEDGEMENTS

This work was supported by grants of the SNSF (105314_152891, CRSII3_141965 and 51NF40_144609) and the SNSF NCCR Affective Sciences to CCR.

CONTRIBUTIONS

MBG, MG, MM, RP and CCR conceived the experiment. MBG, MG, and MM collected andanalysed the data with inputs from RP and CCR. MBG, MG, and CCR wrote the manuscript with inputs from RP and MM.

REFERENCES

1 Ai, C., and Norton, E.C. (2003). Interaction terms in logit and probit models. Economics Letters 80, 123–129.

2 Angrist, J.D., and Pischke, J.-S. (2009). Mostly Harmless Econometrics: An Empiricist's Companion (Princeton, NJ: Princeton University Press).

3 Badre, D., and D'Esposito, M. (2007). Functional Magnetic Resonance Imaging Evidence for a Hierarchical Organization of the Prefrontal Cortex. Journal of Cognitive Neuroscience 19, 2082–2099.

4 Banca, P., Lange, I., Worbe, Y., Howell, N.A., Irvine, M., Harrison, N.A., Moutoussis, M., and Voon, V. (2016). Reflection impulsivity in binge drinking: Behavioural and volumetric correlates. Addiction Biology 21, 504–515.

5 Barbey, A.K., Koenigs, M., and Grafman, J. (2013). Dorsolateral prefrontal contributions to human working memory. Cortex 49, 1195–1205.

6 Basten, U., Biele, G., Heekeren, H.R., and Fiebach, C.J. (2010). How the brain integrates costs and benefits during decision making. Proceedings of the National Academy of Sciences 107, 21767–21772.

7 Berlin, H.A., and Rolls, E.T. (2004). Time Perception, Impulsivity, Emotionality, and Personality in Self-Harming Borderline Personality Disorder Patients. Journal of Personality Disorders 18, 358–378.

8 Bertrand, M., Duflo, E., and Mullainathan, S. (2004). How Much Should We Trust Differences-In-Differences Estimates? The Quarterly Journal of Economics 119, 249–275.

9 Bogacz, R., Brown, E., Moehlis, J., Holmes, P., and Cohen, J.D. (2006). The physics of optimal decision making: A formal analysis of models of performance in two-alternative forced-choice tasks. Psychological Review 113, 700–765.

10 Bogacz, R., Wagenmakers, E.J., Forstmann, B.U., and Nieuwenhuis, S. (2010). The neural basis of the speed-accuracy tradeoff. Trends in Neurosciences 33, 10–16.

11 Brody, C.D., and Hanks, T.D. (2016). Neural underpinnings of the evidence accumulator. Current Opinion in Neurobiology 37, 149–157.

12 Brunton, B.W., Botvinick, M.M., and Brody, C.D. (2013). Rats and Humans Can Optimally Accumulate Evidence for Decision-Making. Science 340, 95–98.

13 Bullier, J., Schall, J.D., and Morel, A. (1996). Functional streams in occipito-frontal connections in the monkey. Behavioural Brain Research 76, 89–97.

14 Busemeyer JR, Townsend JT. (1993). Decision Field-Theory - a Dynamic Cognitive Approach to Decision-Making in an Uncertain Environment. Psychological Review 100: 432-59

15 Cavanagh, J.F., Wiecki, T. v, Cohen, M.X., Figueroa, C.M., Samanta, J., Sherman, S.J., and Frank, M.J. (2011). Subthalamic nucleus stimulation reverses mediofrontal influence over decision threshold. Nature Neuroscience 14, 1462–1467.

16 de Martino, B., Fleming, S.M., Garrett, N., and Dolan, R.J. (2013). Confidence in value-based choice. Nature Neuroscience 16, 105–110.

17 di Lazzaro, V., Pilato, F., Saturno, E., Oliviero, A., Dileone, M., Mazzone, P., Insola, A., Tonali, P.A., Ranieri, F., Huang, Y.Z., et al. (2005). Theta-burst repetitive transcranial magnetic stimulation suppresses specific excitatory circuits in the human motor cortex. The Journal of Physiology 565, 945–950.

18 di Lazzaro, V., Ziemann, U., and Lemon, R.N. (2008). State of the art: Physiology of transcranial motor cortex stimulation. Brain Stimulation 1, 345–362.

19 Ding, L., and Gold, J.I. (2012a). Neural Correlates of Perceptual Decision Making before, during, and after Decision Commitment in Monkey Frontal Eye Field. Cerebral Cortex 22, 1052–1067.

20 Ding, L., and Gold, J.I. (2012b). Separate, Causal Roles of the Caudate in Saccadic Choice and Execution in a Perceptual Decision Task. Neuron 75, 865–874.

21 Domenech, P., and Dreher, J.-C. (2010). Decision Threshold Modulation in the Human Brain. Journal of Neuroscience 30, 14305–14317.

22 Domenech, P., and Koechlin, E. (2015). Executive control and decision-making in the prefrontal cortex. Current Opinion in Behavioral Sciences 1, 101–106.
23 Domenech, P., Redouté, J., Koechlin, E., and Dreher, J.-C. (2017). The Neuro-Computational Architecture of Value-based Selection in the Human Brain. Cerebral Cortex 1–17.
24 Dutilh G, Rieskamp J. (2016). Comparing perceptual and preferential decision making. Psychon Bull Rev 23: 723-37
25 Erlich, J.C., Brunton, B.W., Duan, C.A., Hanks, T.D., and Brody, C.D. (2015). Distinct effects of prefrontal and parietal cortex inactivations on an accumulation of evidence task in the rat. ELife 4.
26 Feltgen, Q., and Daunizeau, J. (2020). Fitting drift-diffusion decision models to trial-by-trial data. BioRxiv.
27 Filimon, F., Philiastides, M.G., Nelson, J.D., Kloosterman, N.A., and Heekeren, H.R. (2013). How Embodied Is Perceptual Decision Making? Evidence for Separate Processing of Perceptual and Motor Decisions. Journal of Neuroscience 33, 2121–2136.
28 Forstmann, B.U., Wagenmakers, E.-J., Eichele, T., Brown, S., and Serences, J.T. (2011). Reciprocal relations between cognitive neuroscience and formal cognitive models: opposites attract? Trends in Cognitive Sciences 15, 272–279.
29 Friston, K.J., Frith, C.D., Liddle, P.F., and Frackowiak, R.S.J. (1993). Functional Connectivity: The Principal-Component Analysis of Large (PET) Data Sets. Journal of Cerebral Blood Flow & Metabolism 13, 5–14.
30 Friston, K.J., Buechel, C., Fink, G.R., Morris, J., Rolls, E., and Dolan, R.J. (1997). Psychophysiological and Modulatory Interactions in Neuroimaging. NeuroImage 6, 218–229.
31 Fuermaier, A.B.M., Hüpen, P., de Vries, S.M., Müller, M., Kok, F.M., Koerts, J., Heutink, J., Tucha, L., Gerlach, M., and Tucha, O. (2018). Perception in attention deficit hyperactivity disorder. ADHD Attention Deficit and Hyperactivity Disorders 10, 21–47
32 Gazzaley, A., Rissman, J., Cooney, J., Rutman, A., Seibert, T., Clapp, W., and D'Esposito, M. (2007). Functional Interactions between Prefrontal and Visual Association Cortex Contribute to Top-Down Modulation of Visual Processing. Cerebral Cortex 17, i125–i135.
33 Glickman, M., Sharoni, O., Levy, D.J., Niebur, E., Stuphorn, V., and Usher, M. (2019). The formation of preference in risky choice. PLoS Computational Biology 15, e1007201.
34 Glimcher, P.W., Kable, J., and Louie, K. (2007). Neuroeconomic Studies of Impulsivity: Now or Just as Soon as Possible? American Economic Review 97, 142–147.
35 Gold JI, Shadlen MN. (2007). The neural basis of decision making. Annual Review of Neuroscience 30: 535-74
36 Goldman-Rakic, P.S., and Leung, H.-C. (2002). Functional Architecture of the Dorsolateral Prefrontal Cortex in Monkeys and Humans (Oxford University Press).
37 Green, N., Biele, G.P., and Heekeren, H.R. (2012). Changes in Neural Connectivity Underlie Decision Threshold Modulation for Reward Maximization. Journal of Neuroscience 32, 14942–14950.
38 Green, N., Bogacz, R., Huebl, J., Beyer, A.K., Kühn, A.A., and Heekeren, H.R. (2013). Reduction of influence of task difficulty on perceptual decision making by stn deep brain stimulation. Current Biology 23, 1681–1684.
39 Grueschow, M., Polania, R., Hare, T.A., and Ruff, C.C. (2015). Automatic versus Choice-Dependent Value Representations in the Human Brain. Neuron 85, 874–885.
40 Grueschow, M., Polania, R., Hare, T.A., and Ruff, C.C. (2018). Arousal Optimizes Neural Evidence Representation for Human Decision-Making. SSRN Electronic Journal.
41 Hanks, T.D., and Summerfield, C. (2017). Perceptual Decision Making in Rodents, Monkeys, and Humans. Neuron 93, 15–31.
42 Hanks, T.D., Kopec, C.D., Brunton, B.W., Duan, C.A., Erlich, J.C., and Brody, C.D. (2015). Distinct relationships of parietal and prefrontal cortices to evidence accumulation. Nature 520, 220–223.
43 Hare, T.A., Camerer, C.F., and Rangel, A. (2009). Self-Control in Decision-Making Involves Modulation of the vmPFC Valuation System. Science 324, 646–648.

44 Heekeren, H.R., Marrett, S., Bandettini, P.A., and Ungerleider, L.G. (2004). A general mechanism for perceptual decision-making in the human brain. Nature 431, 859–862.
45 Heekeren, H.R., Marrett, S., Ruff, D.A., Bandettini, P.A., and Ungerleider, L.G. (2006). Involvement of human left dorsolateral prefrontal cortex in perceptual decision making is independent of response modality. Proceedings of the National Academy of Sciences 103, 10023–10028.
46 Heekeren, H.R., Marrett, S., and Ungerleider, L.G. (2008). The neural systems that mediate human perceptual decision making. Nature Reviews Neuroscience 9, 467–479.
47 Heng, J.A., Woodford, M., and Polania, R. (2020). Efficient sampling and noisy decisions. Elife 9.
48 Herz, D.M., Zavala, B.A., Bogacz, R., and Brown, P. (2016). Neural Correlates of Decision Thresholds in the Human Subthalamic Nucleus. Current Biology 26, 916–920.
49 Herz, D.M., Tan, H., Brittain, J.S., Fischer, P., Cheeran, B., Green, A.L., Fitzgerald, J., Aziz, T.Z., Ashkan, K., Little, S., et al. (2017). Distinct mechanisms mediate speed-accuracy adjustments in cortico-subthalamic networks. ELife 6, 1–25.
50 Heyes, S.B., Adam, R.J., Urner, M., van der Leer, L., Bahrami, B., Bays, P.M., and Husain, M. (2012). Impulsivity and rapid decision-making for reward. Frontiers in Psychology 3, 1–11.
51 Huang, Y.Z., Edwards, M.J., Rounis, E., Bhatia, K.P., and Rothwell, J.C. (2005). Theta burst stimulation of the human motor cortex. Neuron 45, 201–206.
52 Hutcherson, C.A., Bushong, B., and Rangel, A. (2015). A Neurocomputational Model of Altruistic Choice and Its Implications. Neuron 87, 451–462.
53 Karaca-Mandic, P., Norton, E.C., and Dowd, B. (2012). Interaction terms in nonlinear models. Health Services Research 47, 255–274.
54 Kiani, R., Corthell, L., and Shadlen, M.N. (2014). Choice certainty is informed by both evidence and decision time. Neuron 84, 1329–1342.
55 Kim JN, Shadlen MN. (1999). Neural correlates of a decision in the dorsolateral prefrontal cortex of the macaque. Nature Neuroscience 2: 176-85.
56 Knecht, S., Ellger, T., Breitenstein, C., Ringelstein, E.B., and Henningsen, H. (2003). Changing cortical excitability with low-frequency transcranial magnetic stimulation can induce sustained disruption of tactile perception. Biological Psychiatry 53, 175–179.
57 Koechlin, E., and Summerfield, C. (2007). An information theoretical approach to prefrontal executive function. Trends in Cognitive Sciences 11, 229–235.
58 Krajbich I. (2019). Accounting for attention in sequential sampling models of decision making. Curr Opin Psychol 29: 6-11
59 Liu, T., and Pleskac, T.J. (2011). Neural correlates of evidence accumulation in a perceptual decision task. 48824, 2383–2398.
60 Logothetis, N.K. (2008). What we can do and what we cannot do with fMRI. Nature 453, 869–878.
61 Mawase, F., Lopez, D., Celnik, P.A., and Haith, A.M. (2018). Movement repetition facilitates response preparation. Cell Reports 24, 801–808.
62 Mulder MJ, van Maanen L, Forstmann BU. (2014). Perceptual decision neurosciences - a model-based review. Neuroscience 277: 872-84
63 Murd, C., Moisa, M., Grueschow, M., Polania, R., and Ruff, C.C. (2020). Causal contributions of human frontal eye fields to distinct aspects of decision formation. Scientific Reports 10, 7317.
64 Nee, D.E., and D'Esposito, M. (2016). The hierarchical organization of the lateral prefrontal cortex. ELife 5.
65 Owen, A.M. (1997). The Functional Organization of Working Memory Processes Within Human Lateral Frontal Cortex: The Contribution of Functional Neuroimaging. European Journal of Neuroscience 9, 1329–1339.
66 Palmeri, T.J., Love, B.C., and Turner, B.M. (2017). Model-based cognitive neuroscience. Journal of Mathematical Psychology 76.

67 Peters, J., and D'Esposito, M. (2020). The drift diffusion model as the choice rule in inter-temporal and risky choice: a case study in medial orbitofrontal cortex lesion patients and controls. PLoS Computational Biology 16, e1007615.
68 Petrides, M. (2005). Lateral prefrontal cortex: architectonic and functional organization. Philosophical Transactions of the Royal Society B: Biological Sciences 360, 781–795.
69 Philiastides, M.G., Auksztulewicz, R., Heekeren, H.R., and Blankenburg, F. (2011). Causal role of dorsolateral prefrontal cortex in human perceptual decision making. Current Biology 21, 980–983.
70 Piet AT, Erlich JC, Kopec CD, Brody CD. (2017). Rat Prefrontal Cortex Inactivations during Decision Making Are Explained by Bistable Attractor Dynamics. Neural Comput 29: 2861-86
71 Plummer, M. (2016) rjags: Bayesian graphical models using MCMC. R package version, 4(6).
72 Polanía, R., Krajbich, I., Grueschow, M., and Ruff, C.C. (2014). Neural Oscillations and Synchronization Differentially Support Evidence Accumulation in Perceptual and Value-based Decision Making. Neuron 82, 709–720.
73 Polania R, Moisa M, Opitz A, Grueschow M, Ruff CC. (2015). The precision of value-based choices depends causally on fronto-parietal phase coupling. Nat Commun 6
74 Poldrack, R. (2006). Can cognitive processes be inferred from neuroimaging data? Trends in Cognitive Sciences 10, 59–63.
75 Postle, B.R. (2016). How Does the Brain Keep Information "in Mind"? Current Directions in Psychological Science 25, 151–156.
76 Puhani, P.A. (2012). The treatment effect, the cross difference, and the interaction term in nonlinear "difference-in-differences" models. Economics Letters 115, 85–87.
77 Rahnev, D., Nee, D.E., Riddle, J., Larson, A.S., and D'Esposito, M. (2016). Causal evidence for frontal cortex organization for perceptual decision making. Proceedings of the National Academy of Sciences 113, 6059–6064.
78 Ramsey, J.D., Hanson, S.J., Hanson, C., Halchenko, Y.O., Poldrack, R.A., and Glymour, C. (2010). Six problems for causal inference from fMRI. NeuroImage 49, 1545–1558.
79 Ratcliff R, Rouder JN. (1998). Modeling response times for two-choice decisions. Psychol Sci 9: 347-56
80 Ratcliff, R. and Smith, P. (2004) A comparison of sequential sampling models for two-choice reaction time. Psychological Review 111(2): 333-367.
81 Ratcliff, R. and McKoon, G. (2004) The diffusion decision model: theory and data for two choice-decision tasks. Neural Computation 20(4): 873-922.
82 Ratcliff, R., and McKoon, G. (2008). The Diffusion Decision Model: Theory and Data for Two-Choice Decision Tasks. Neural Computation 20, 873–922.
83 Serences, J.T., Ester, E.F., Vogel, E.K., and Awh, E. (2009). Stimulus-Specific Delay Activity in Human Primary Visual Cortex. Psychological Science 20, 207–214.
84 Shadlen, M.N., and Newsome, W.T. (1996). Motion perception: seeing and deciding. Proceedings of the National Academy of Sciences 93, 628–633.
85 Sokol-Hessner, P., Hutcherson, C., Hare, T., and Rangel, A. (2012). Decision value computation in DLPFC and VMPFC adjusts to the available decision time. European Journal of Neuroscience 35, 1065–1074.
86 Smith PL, Ratcliff R. (2004). Psychology and neurobiology of simple decisions. Trends Neurosci 27: 161-68
87 Starns, J.J., and Ma, Q. (2018). Response biases in simple decision making: Faster decision making, faster response execution, or both? Psychonomic Bulletin & Review 25, 1535–1541.
88 Summerfield C, Tsetsos K. (2012). Building bridges between perceptual and economic decision-making: neural and computational mechanism. Front Neurosci-Switz 6
89 Tajima S, Drugowitsch J, Pouget A. (2016). Optimal policy for value-based decision-making. Nat Commun 7: 12400.
90 Thut, G., and Pascual-Leone, A. (2010). A review of combined TMS-EEG studies to characterize lasting effects of repetitive TMS and assess their usefulness in cognitive and clinical neuroscience. Brain Topography 22, 219–232.

91 Tosoni, A., Galati, G., Romani, G.L., and Corbetta, M. (2008). Sensory-motor mechanisms in human parietal cortex underlie arbitrary visual decisions. Nature Neuroscience 11, 1446–1453.
92 Turner, B.M., van Maanen, L., and Forstmann, B.U. (2015). Informing cognitive abstractions through neuroimaging: the neural drift diffusion model. Psychological Review 122, 312–336.
93 Usher M, McClelland JL. (2001). The time course of perceptual choice: The leaky, competing accumulator model. Psychological Review 108: 550-92
94 Vandekerckhove, J., Tuerlinckx, F., and Lee, M.D. (2011). Hierarchical diffusion models for two-choice response times. Psychological Methods 16, 44–62.
95 White, C.N., Servant, M., and Logan, G.D. (2018). Testing the validity of conflict drift-diffusion models for use in estimating cognitive processes: A parameter-recovery study. Psychonomic Bulletin & Review 25, 286–301.
96 Wycoco, V., Shroff, M., Sudhakar, S., and Lee, W. (2013). White Matter Anatomy. Neuroimaging Clinics of North America 23.
97 Wijeakumar, S., Ambrose, J.P., Spencer, J.P., and Curtu, R. (2017). Model-based functional neuroimaging using dynamic neural fields: An integrative cognitive neuroscience approach. Journal of Mathematical Psychology 76, 212–235.
98 Zanto, T.P., Rubens, M.T., Thangavel, A., and Gazzaley, A. (2011). Causal role of the prefrontal cortex in top-down modulation of visual processing and working memory. Nature Neuroscience 14, 656–661.

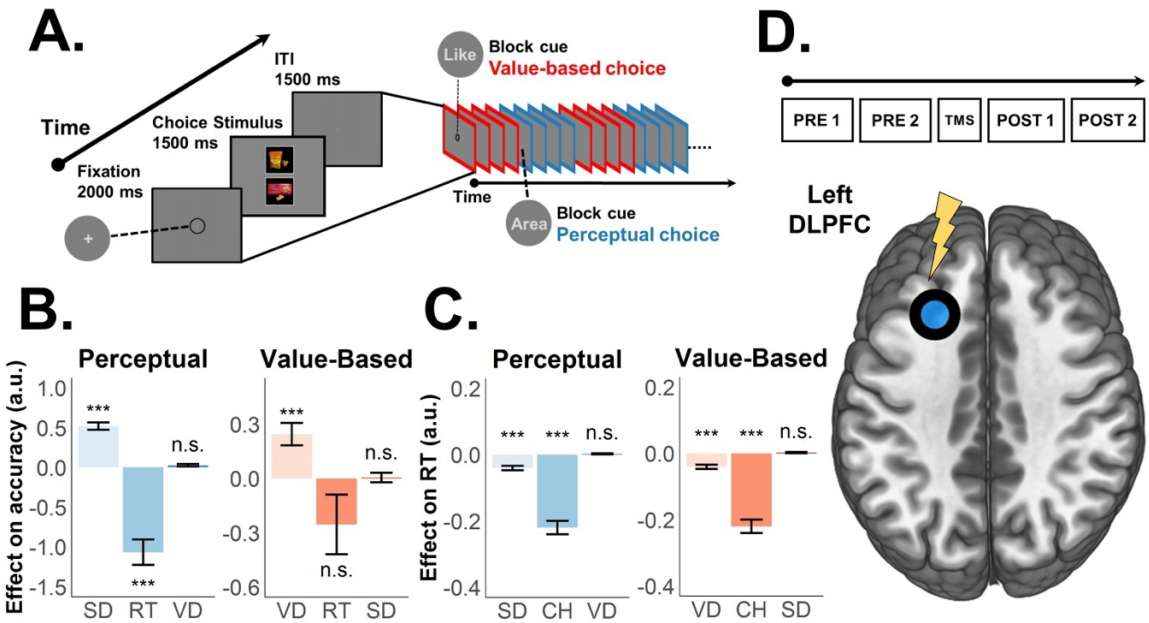

Figure 1. Behavioural food choice paradigm, theta-burst stimulation protocol, and behavioural regressions. (a) Example of decision stage. Participants were cued in advance about the type of decision required. Perceptual decisions required participants to choose the food item with the largest size while value-based decisions required participants to choose the food item they preferred to consume at the end of the experiment. Participants alternated between blocks of perceptual (blue) or value-based (red) choice trials (7-9 trials per task-block). **(b)** Logistic regression results show that the larger the evidence strength, the more likely decision makers will respond accurately. Choice accuracy is only related to the evidence that is currently task-relevant (size difference SD for perceptual or value difference VD for value-based choice), not to the task-irrelevant evidence (RT is reaction time of current choice). **(c)** Similarly, our linear regressions show that RTs are negatively associated only with the task-relevant evidence (and lower for perceptual choices overall, captured by regressor CH (1 = perceptual, 0 = value-based)). Consistent with previous findings, the results in (b) and (c) confirm that our paradigm can distinguish and compare evidence processing for matched perceptual- and value-based decisions. Error bars in (b) and (c) represent the 95% confidence interval range of the estimated effect sizes. * $p < 0.05$, ** $p < 0.01$, and *** $p < 0.001$. **(d)** Theta-burst stimulation protocol. After the fourth pre-TMS run, participants received continuous theta-burst stimulation (cTBS) over the left SFS region of interest (ROI) (area encircled and colored blue). cTBS consisted of 200 trains of 600 pulses of 5 Hz frequency for 50 s.

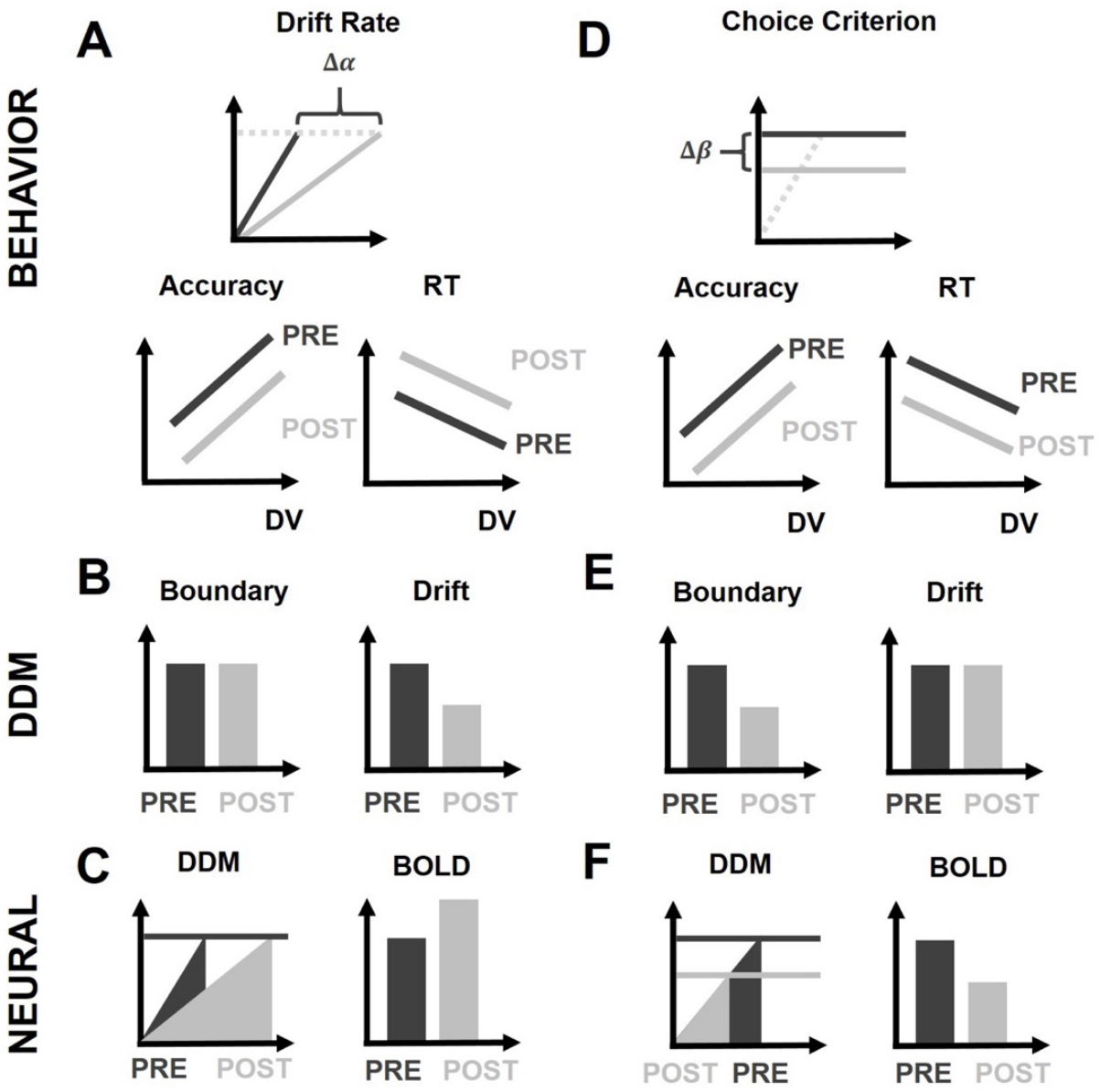

Figure 2. Study hypotheses. Scenario 1: left SFS is causally involved in evidence accumulation. Theta-burst induced inhibition of left SFS should lead to reduced evidence accumulation (a), expressed as lower accuracy (a, 2nd row, left), slowing of RTs (a, 2nd row, right), and a reduction of DDM drift rate (b, right) without any effect on the boundary parameter (b, left). Since the neural activity devoted to evidence accumulation (area under the curve) should increase (c, left), we would expect higher BOLD signal in this case (c, right). Scenario 2: left SFS is causally involved in setting the choice criterion. Theta-burst induced inhibition of left SFS should lead to a lower choice criterion (d), expressed as lower choice accuracy (d, 2nd row, left), faster RTs (d, 2nd row, right), and a reduced DDM decision boundary parameter (e, left) without any effect on the DDM drift-rate (e, right). At the neural level, we should observe reduced BOLD activity due to the lower amount of evidence processed by the neurons (f, right), and reflected by the smaller area under the evidence-accumulation curve when it reaches the lower boundary (f, left).

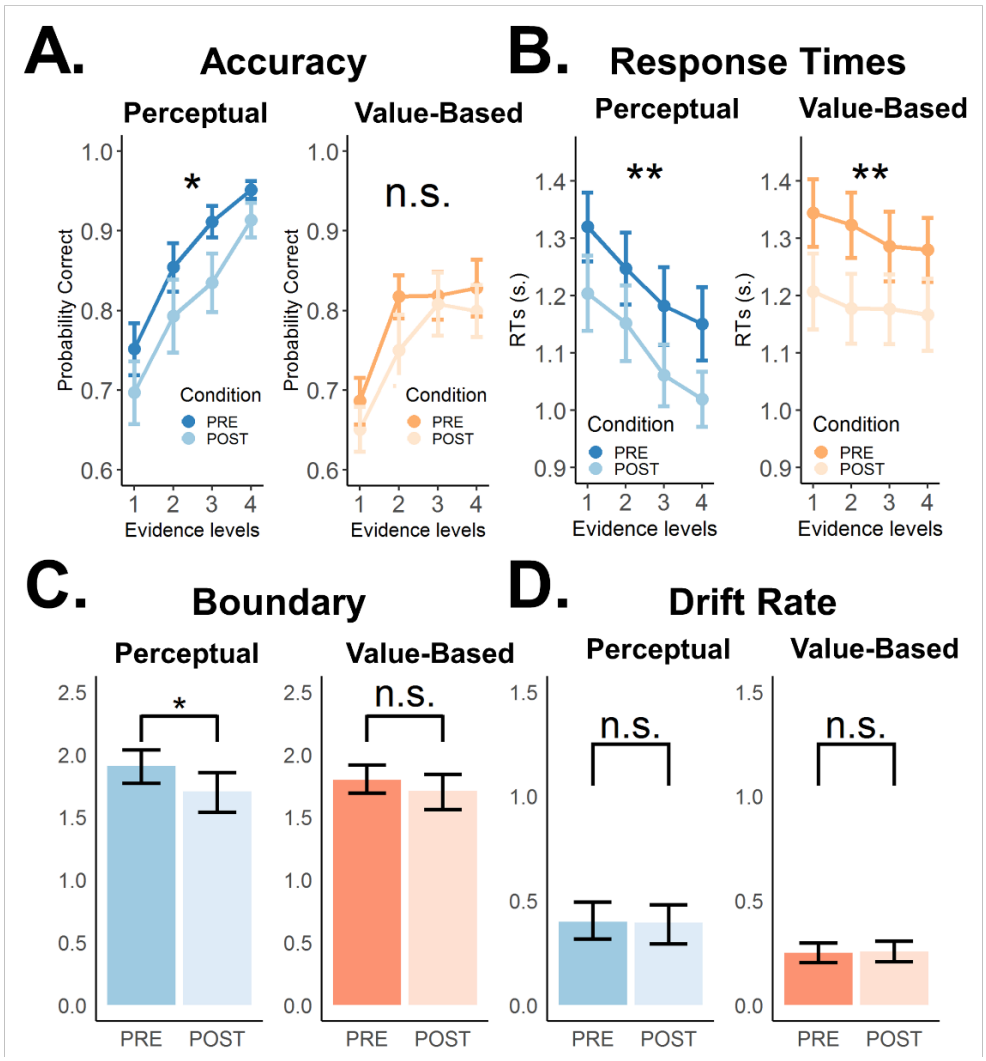

Figure 3. Theta-burst stimulation over the left SFS affects choice behavior and selectively lowers the decision boundary for perceptual but not value-based choices. (a) Choice accuracies/ consistencies and **(b)** response times (RTs) for perceptual (blue) and value-based (orange) decisions for different evidence levels during pre-cTBS (dark) and post-cTBS (light) stimulation periods. Error bars in (a) and (b) represent s.e.m. Consistent with previous findings, stronger evidence leads to more accurate choices and faster RTs in both types of decisions. Importantly, theta-burst stimulation significantly lowered choice accuracy selectively for perceptual, not value-based decisions (negative main stimulation effect for perceptual decisions and negative stimulation × task interaction; **Supplementary Fig. 2c** and see also **Supplementary Fig. 2a** for changes in choice accuracy across runs). Additionally, theta-burst stimulation also significantly lowered RTs in both choice types (negative main stimulation effect; **Supplementary Fig. 2c** and see also **Supplementary Fig. 2b** for changes in RTs across runs). **(c)** Theta-burst stimulation selectively decreased the decision boundary in perceptual decisions only (difference between estimated posterior population distributions; see **Methods** and **Supplementary Fig. 5a** for a detailed post-hoc analysis). All the other parameters, particularly **(d)** the drift rate (see also **Supplementary Fig. 5b** for post-hoc analysis) remain unaffected by stimulation. Error bars in (c) and (d) represent the 95% confidence interval range of the posterior estimates of the DDM parameters. * $p < 0.05$, ** $p < 0.01$, and *** $p < 0.001$.

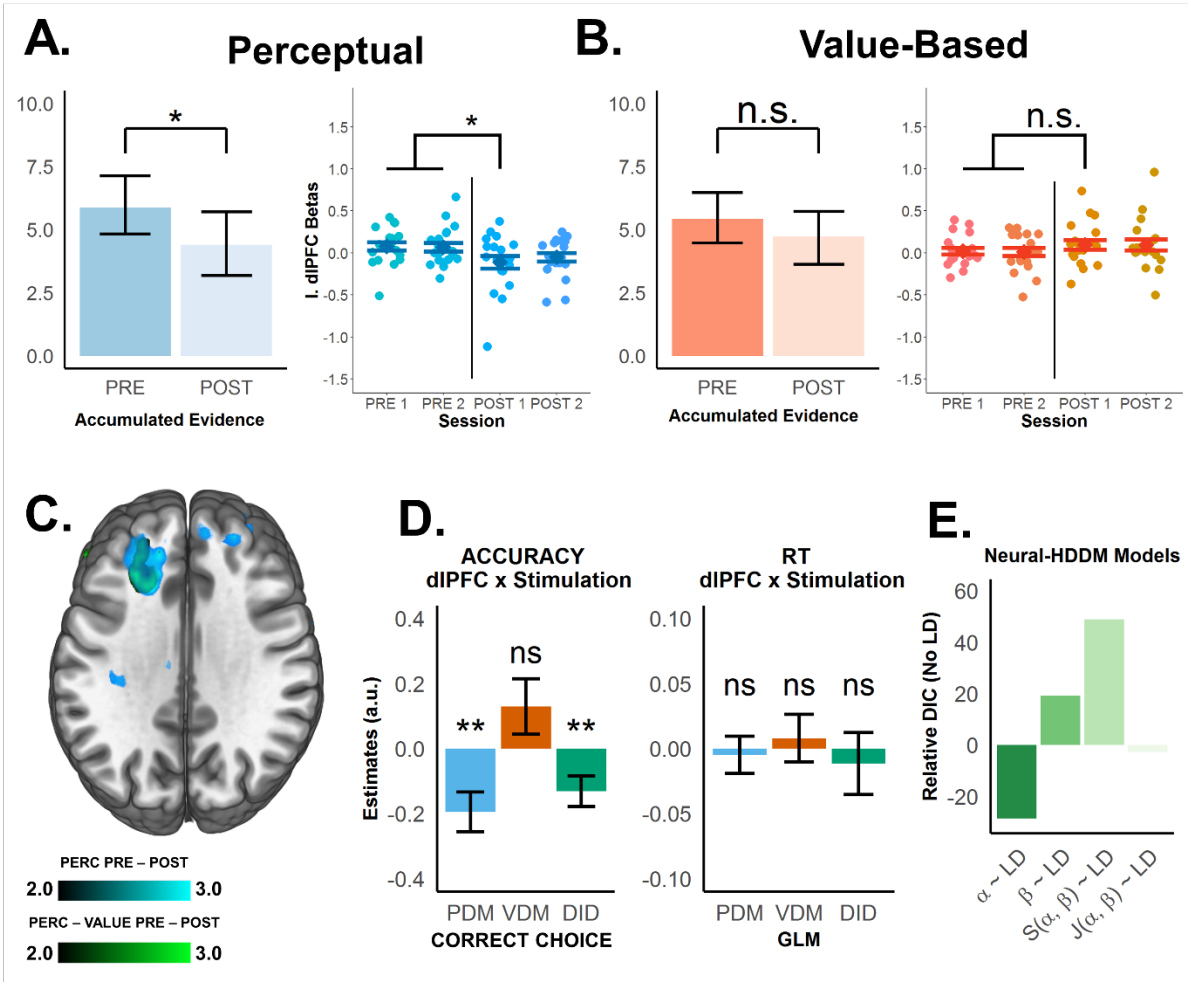

Figure 4. Neural representation of accumulated evidence in the left SFS is disrupted after theta-burst stimulation, and is linked with behavior and neural computation. (a) Left panel: Accumulated evidence (AE) simulation derived from the fitted DDM (left panel). Previous studies have illustrated how the accumulation-to-bound process convolved with the hemodynamic response function (HRF) results in BOLD signals; hence, the simulated AE provides a suitable prediction of BOLD responses in brain regions involved in evidence accumulation. Theta-burst stimulation selectively decreased AE for (a) perceptual (blue), not **(b)** value-based (orange) decisions (see **Supplementary Fig. 6b** for post-hoc analysis). We constructed a trialwise measure of accumulated evidence using RTs and evidence strength for our parametric modulator (see **Methods**). Individual ROIs extracted from the left SFS representing accumulated evidence across runs (right panels; see **Methods**) show that consistent with the DDM prediction, theta-burst stimulation selectively decreased BOLD response representing AE in left SFS during perceptual, not value-based decisions. Error bars in the left panels of (a) and (b) represent the 95% confidence interval range of the posterior estimates of the DDM parameters, while error bars in their respective right panels represent s.e.m. **(c)** Post–pre contrasts for the trialwise accumulated-evidence regressor show reduced left-SFS BOLD during perceptual decisions (green overlay), with a significantly stronger reduction for perceptual vs value-based decisions (blue overlay). No reduction is observed for value-based decisions. **(d)** To test the link between neural and behavioural effects of TMS, regression results show that after stimulation, BOLD changes in left SFS are associated with lower choice accuracy (left panel) for perceptual (PDM, blue) (negative left SFS × stimulation interaction) but not value-based choices (VDM, red), with significant differences between the effects on both choice types (difference-in-difference, DID, green,

negative left SFS × stimulation × task interaction). On the other hand, cTBA-induced changes in left SFS activity are unrelated to changes in RT (right panel). Error bars in (d) represent the 95% confidence interval range of the estimated effect sizes. * $p < 0.05$, ** $p < 0.01$, and *** $p < 0.001$. **(e)** To test the link between neural activity and DDM computations, we included trialwise beta estimates of left-SFS BOLD signals as inputs to the DDM. Alternative models tested whether trialwise left-SFS (LD) activity modulates the decision boundary (α) (**Model 1**), the drift rate (β), or a combination of both (**Models 3** and **4**, see **Methods** and **Supplementary Fig. 8** for more details). Model comparisons using the deviance information criterion (**DIC**, smaller values mean better fits) showed that Model 1 fits the data best, confirming that the left SFS is involved in selectively changing the decision boundary for perceptual decisions.

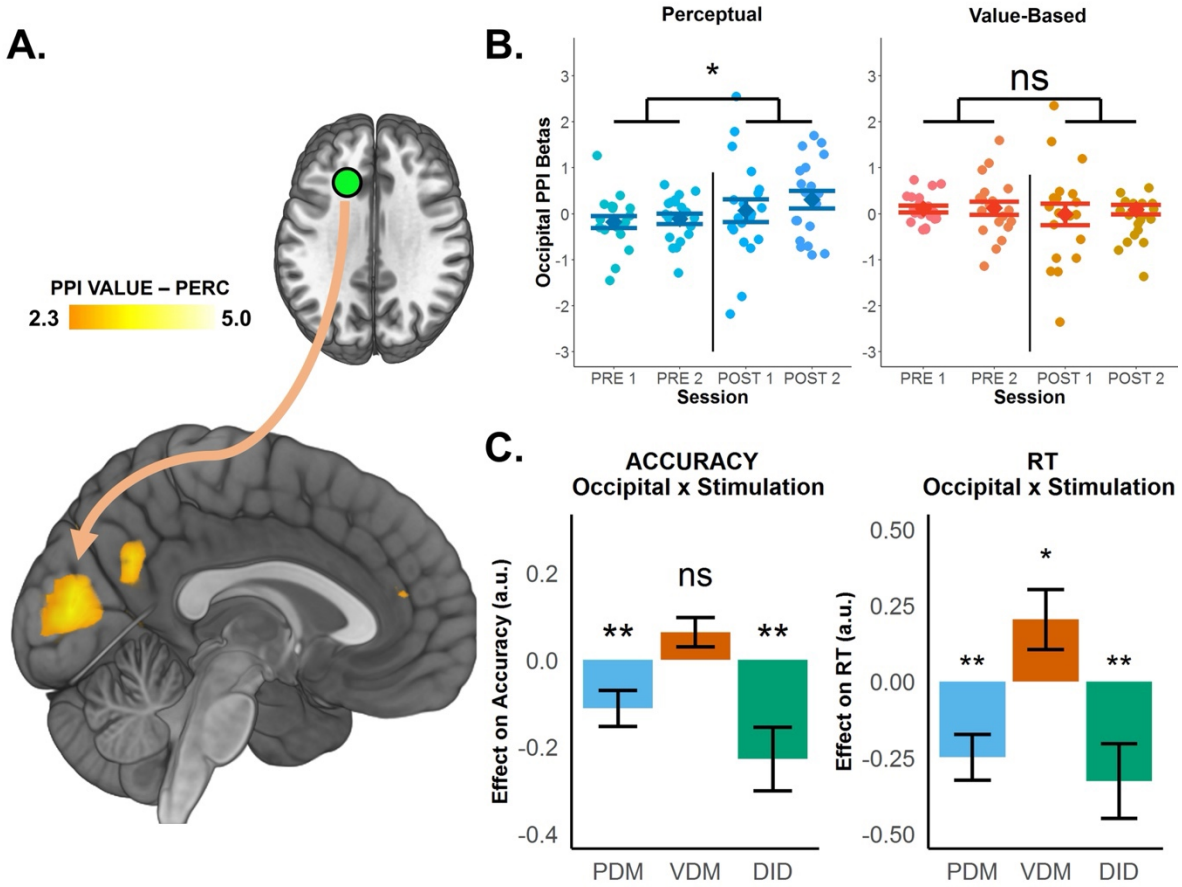

Figure 5. SFS-TMS-related changes in behaviour and neural computations are accompanied by increased functional coupling between the left SFS and occipital cortex. (a) Psychophysiological interaction (PPI) analysis reveals an area in occipital cortex showing increased functional coupling with the left SFS during perceptual choices. **(b)** ROI analysis of individual PPI betas shows that *aE*-related functional coupling between the left SFS and OCC is selectively increased post stimulation during perceptual (left panel) but not value-based decisions (right panel). Error bars in (b) represent s.e.m. **(c)** Regression results testing the link between cTBS effects on left SFS-OCC functional coupling and behaviour. Increased SFS-OCC coupling is associated with lower choice accuracy (left panel) specifically for perceptual (PDM, blue, negative OCC × stimulation interaction) but not value-based choices (VDM, red). In addition, increased functional coupling is also associated with faster RTs (right panel) for perceptual (blue, negative OCC × stimulation interaction) and slower RTs for value-based choice (red, positive OCC × stimulation interaction). Error bars in (c) represent the 95% confidence interval range of the estimated effect sizes. * $p < 0.05$, ** $p < 0.01$, and *** $p < 0.001$.

SUPPLEMENTARY MATERIAL

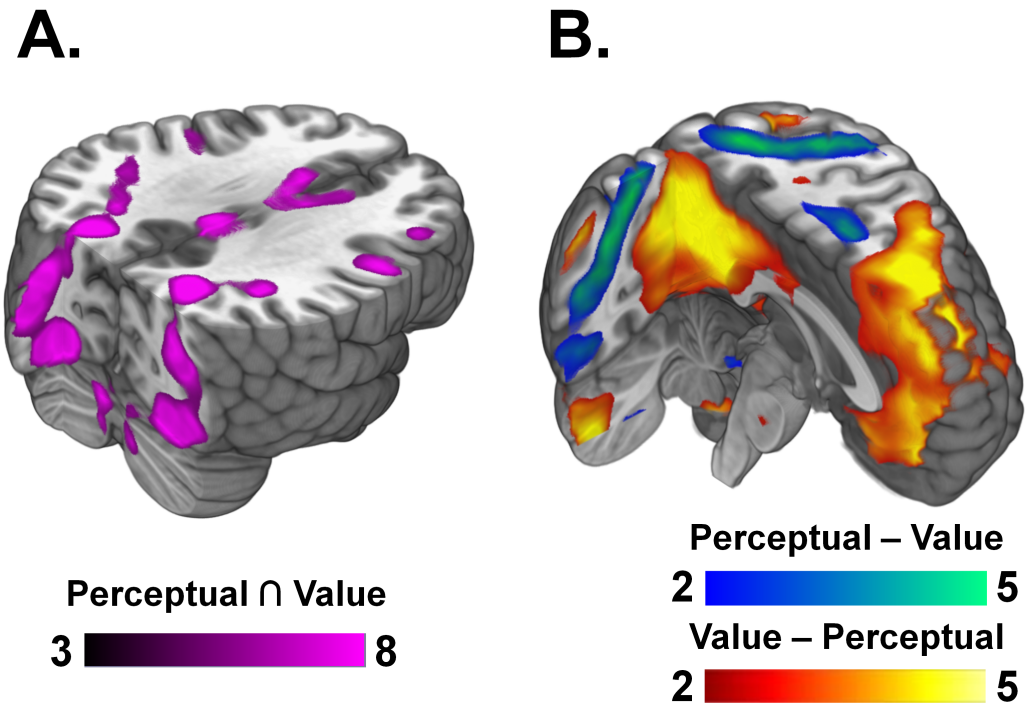

Supplementary Figure 1. Domain-general and domain-specific regions involved in perceptual and value-based decisions. (a) Domain-general regions. We found domain-general regions shared by both perceptual decision making (PDM) and value-based decision making (VDM), such as areas in the visual stream along the fusiform gyrus, cerebellar areas including the brainstem and motor areas such as premotor cortex and SMA (conjunction a $p < 0.05$, cluster-corrected, see **Supplementary Table 1** for the complete list of regions). **(b)** Domain-specific regions. Comparing average decision-related activity between perceptual and value-based decisions revealed distinct brain activations. Blue-green represents significant neural activity for PDM > VDM decisions while red-yellow represents significant activity for VDM > PDM (see **Supplementary Table 2**). Among the active regions in the VDM > PDM contrast include the orbitofrontal cortex, the posterior cingulate cortex, and the media prefrontal cortex while the regions active in the PDM > VDM contrast include the frontal eye fields, the intraparietal sulcus and premotor cortex.

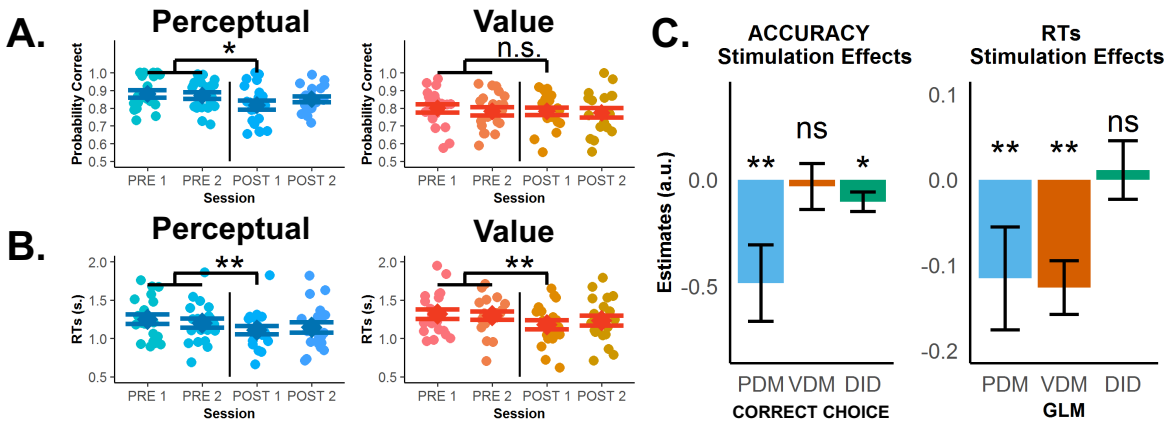

Supplementary Figure 2. Theta-burst stimulation in left SFS selectively lowers choice accuracy for perceptual decisions, but RTs become faster after stimulation in both choice types. (a) Observed accuracies and **(b)** mean RTs of individual participants for perceptual decision making, PDM (blue) and value-based decision making, VDM (orange-yellow) across pre-stimulation and post-stimulation runs. Error bars in (a) and (b) represent s.e.m. Theta-burst stimulation significantly lowered choice accuracy for PDM, not VDM, especially during the first post-stimulation run. On the other hand, RTs sped up in both perceptual and value-based decisions. Unsurprisingly, both accuracy levels and RTs began to recover during the second post-stimulation run for PDM. **(c)** In our regression analysis, comparing the pre-post PDM difference in accuracy with the pre-post VDM difference confirm the significant effect of theta-burst stimulation in selectively lowering choice accuracy (left panel) for perceptual decisions (green, negative stimulation × task interaction). In contrast, the effect is nonspecific for RTs (right panel). Error bars in (c) represent the 95% confidence interval range of the estimated effect sizes. * $p < 0.05$, ** $p < 0.01$, and *** $p < 0.001$.

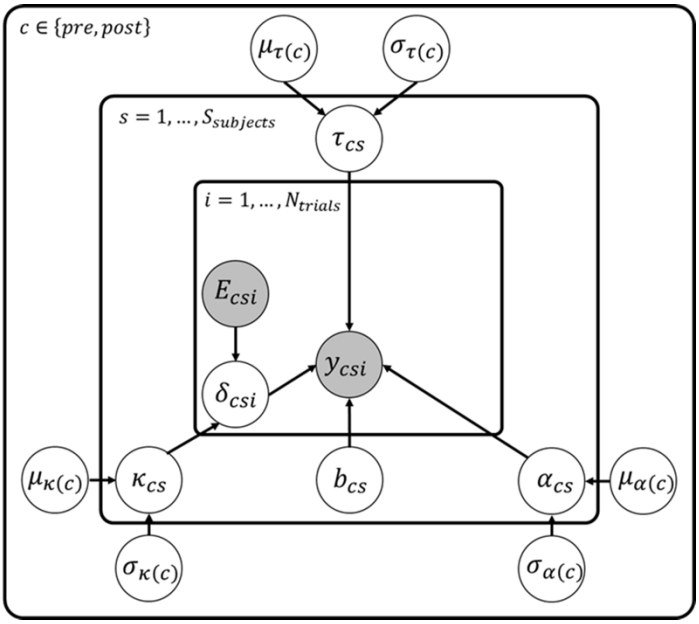

Supplementary Figure 3. Hierarchical Bayesian DDM. Graphical representation of the hierarchical Bayesian DDM fitted to choice data. Clear circles represent latent variables while filled circles represent observed variables, i.e. choice data, y, and evidence, E, for each trial i. Choice data contain both accuracy and response times. The following equations show the distributions assumed for each of the latent variables in the model:

Trial-by-trial, i

$$y_{c,s,i} \sim Wiener\left(a_{cs}, \beta, \tau_{c,s}, \delta_{c,s,i}\right)$$

$$\delta_{c,s,i} = \kappa_{c,s} \times E_{c,s,i}$$

Subject, c

$$a_{c,s} \sim \mathbb{N}\left(\mu_{\alpha}(c), \sigma^2_{\alpha(c)}\right)$$

$$\tau_{c,s} \sim \mathbb{N}\left(\mu_{\tau}(c), \sigma^2_{\tau(c)}\right)$$

$$\kappa_{c,s} \sim \mathbb{N}\left(\mu_{\kappa}(c), \sigma^2_{\kappa(c)}\right)$$

$$b_{c,s} = 0.5$$

Observable variables

$$y_{c,s,i} = \begin{cases} rt_{c,s,i}, & correct = 1 \\ -rt_{c,s,i}, & correct = 0 \end{cases}$$

$$E = \{V_{best} - V_{worst}\} \; or \; \{S_{biggest} - S_{smallest}\}$$

For the hyper-group or latent parameters at the highest level of the hierarchy (represented by μ_x and σ_x), we assumed flat uniform priors. The distributions for the following are:

$$\kappa \sim U(-8,8), \qquad \alpha \sim U(0.001,5), \qquad \kappa \sim U(0.01,2)$$

The following model parameters are: α (decision threshold), κ (drift rate parameter scaling the evidence, E), and τ (nondecision times).

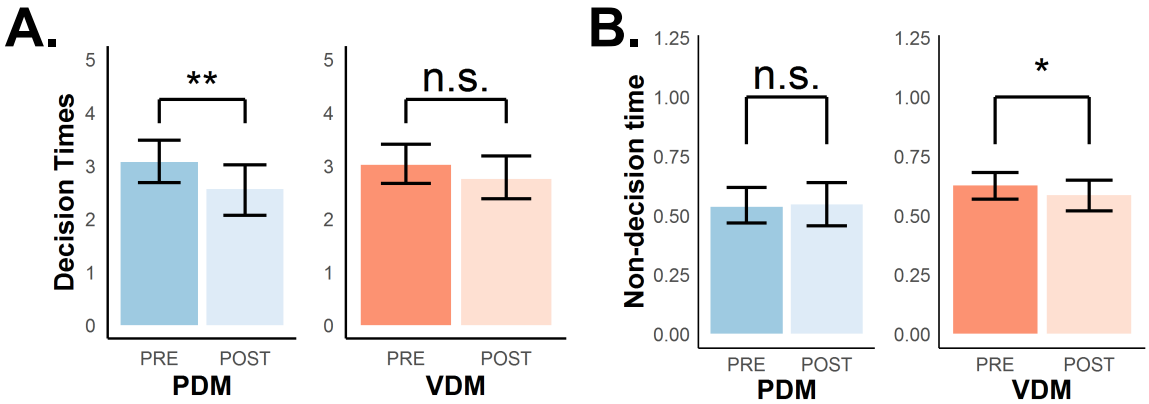

Supplementary Figure 4. The DDM disentangles the latent decision-relevant and decision-irrelevant processes observed with faster RTs. (a) We derived a measure of decision times (DT, upper row) and **(b)** estimated non-decision times (nDT, lower row) from the DDM. We derived and estimated these parameters to test whether faster RTs in both perceptual decision making (PDM) and value-based decision making (VDM) after stimulation is due to the same or different latent processes in the DDM, and whether these processes are decision-relevant or not. These results show that different latent processes are driving faster RTs for PDM and VDM. Theta-burst stimulation significantly lowered decision times in perceptual (blue), not value-based (orange) decisions. In contrast, stimulation marginally but selectively decreased nondecision times for VDM, not PDM. A Post-hoc analysis confirms domain-specificity of lower nDT for VDM (**Supplementary Fig. 5c**). Taken together, these results explain what processes underlie observed faster RTs in both decisions. Error bars represent the 95% confidence interval range of the posterior estimates of the DDM parameters. * $p < 0.05$, ** $p < 0.01$, and *** $p < 0.001$.

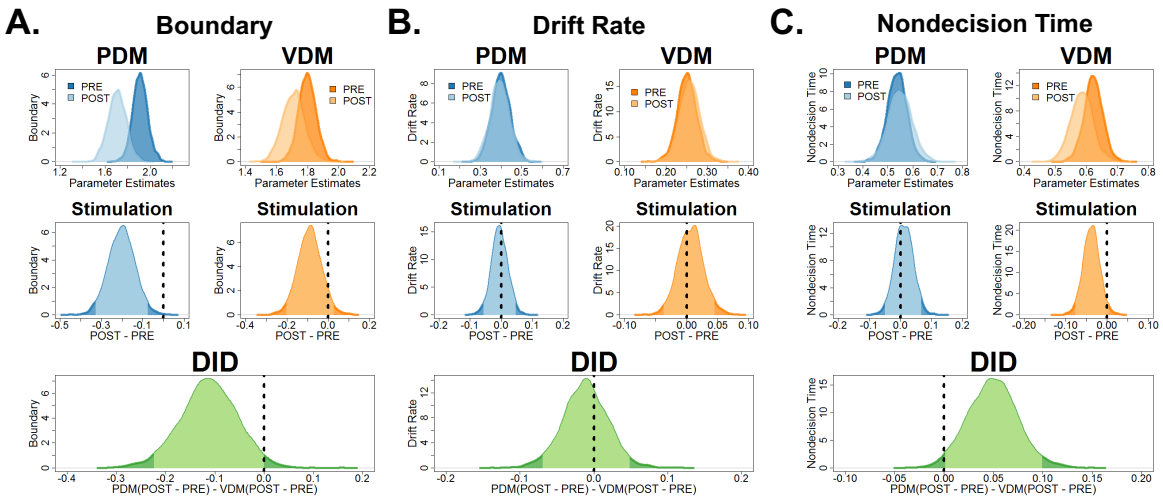

Supplementary Figure 5. Theta-burst stimulation in the left SFS reduced decision boundary for perceptual decisions. (a) Bayesian poster probability distributions of DDM parameters (top row of panel) before (dark color) and after stimulation (light color) for perceptual (blue) and value-based (yellow-orange) decisions. Theta-burst stimulation has lowered the decision boundary for perceptual decision (PDM) not value-based decisions (VDM). **(b)** Drift-rate was unaffected after theta-burst stimulation, while **(c)** nondecision times decreased in VDM, not PDM. To test for a stimulation effect, post-hoc tests (middle row of panel) compare pre- and post-stimulation DDM parameters for each type of decision. The highest density interval (HDI) spans within the 95% interval (light color) and represents a null effect. We can statistically confirm the effect of theta-burst stimulation if the decision criterion (dashed vertical line) is outside the 95% HDI (dark color). In our post-hoc analysis, only the decision boundary during PDM had its criterion outside the 95% HDI and marginally for nondecision times. However, the criterion for the drift rate was well within the 95% HDI. Hence, these results show that theta-burst stimulation significantly decreased the decision boundary for PDM and nondecision times for VDM. To test whether stimulation is selective for only one decision domain, our post-hoc test (green, bottom row) compared the pre-post PDM differences with the pre-post VDM differences. In this analysis, both the criterion for the decision boundary and nondecision times were outside the 95% HDI.

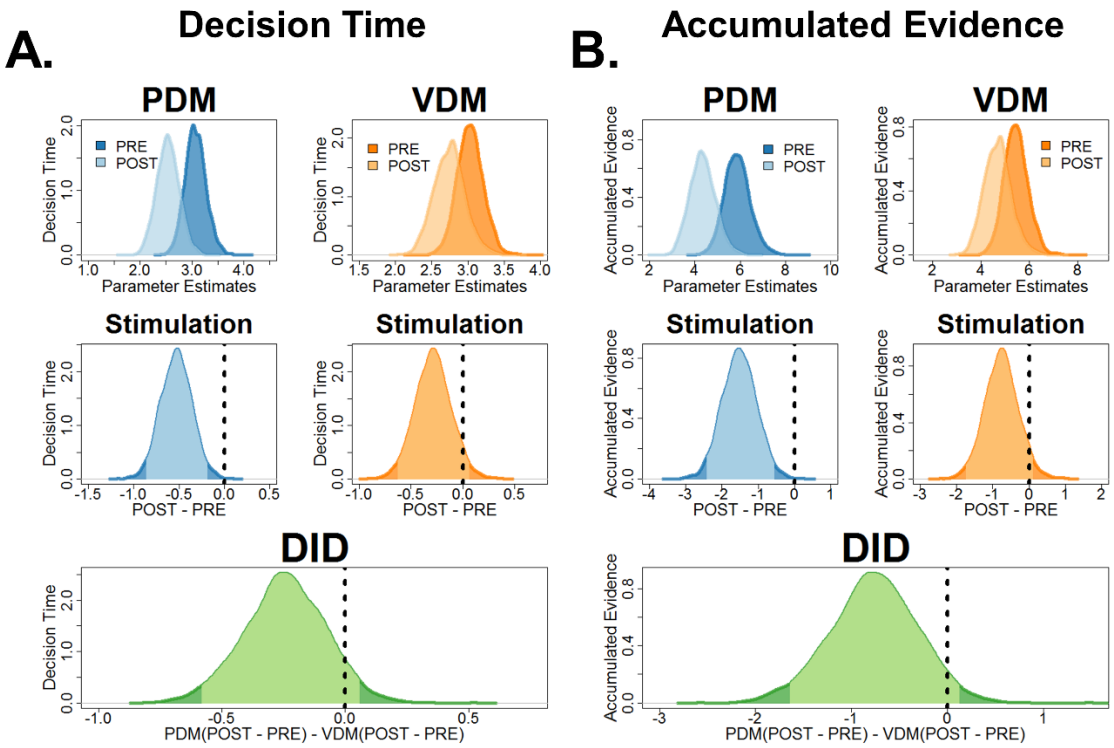

Supplementary Figure 6. Simulations of fitted model: Theta-burst stimulation in the left SFS reduced decision times and accumulated evidence. (a) Bayesian posterior probability distributions (top row) of decision times and **(b)** accumulated evidence before (dark color) and after (light color) for perceptual (blue) and value-based (yellow-orange) decisions. Post-hoc tests (middle row) comparing pre- and post-stimulation revealed that theta-burst stimulation significantly decreased both decision times and accumulated evidence for perceptual, not value-based decisions. However, post-hoc tests comparing the pre-post PDM differences with the pre-post VDM differences showed that the criterion is marginally inside the 95% HDI.

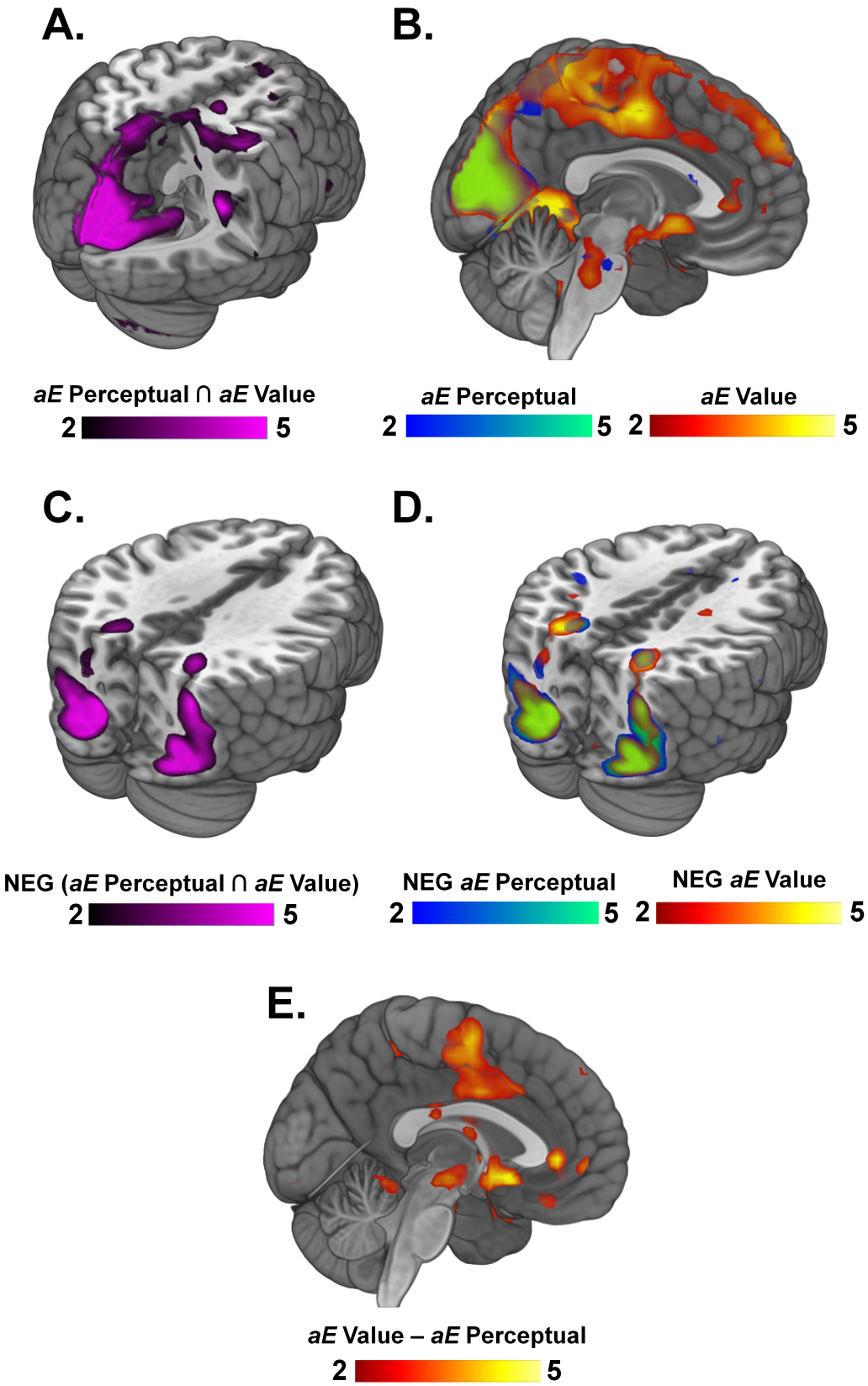
A.
B.
aE Perceptual ∩ aE Value
2
5
aE Perceptual
2
5
aE Value
2
5
C.
D.
NEG (aE Perceptual ∩ aE Value)
2
5
NEG aE Perceptual
2
5
NEG aE Value
2
5
E.
aE Value – aE Perceptual
2
5

1402

Supplementary Figure 7. Neural representations of accumulated evidence across the whole brain for PDM and VDM. (a) Conjunction between areas representing accumulated evidence (*aE*) during perceptual (PDM) and value-based decisions (VDM) reveals activations in visual and parietal areas, such as the cuneus, postcentral gyrus, and lingual gyrus (see **Supplementary Table 3**). **(b)** Representations of accumulated evidence for PDM and VDM. Particularly, BOLD responses associated with AE in perceptual decisions are seen in the left SFS (see **Supplementary Table 3**). **(c)** Negative conjunction contrasts shared by both PDM and VDM represent the efficiency of evidence accumulation (i.e., the inverse of accumulated evidence). These contrasts reveal activations in occipital and parietal areas (see **Supplementary Table 3**). Particularly, parietal areas have been previously implicated in the efficiency of accumulating evidence. **(d)** Negative contrasts for each choice domain reveal activations in parietal and occipital areas (see **Supplementary Table 4**). **(e)** Contrasts comparing the neural representation of accumulated evidence between value-based and perceptual decisions revealed activations in areas such as the ventromedial prefrontal cortex (vmPFC) and the nucleus accumbens (see **Supplementary Table 4**).

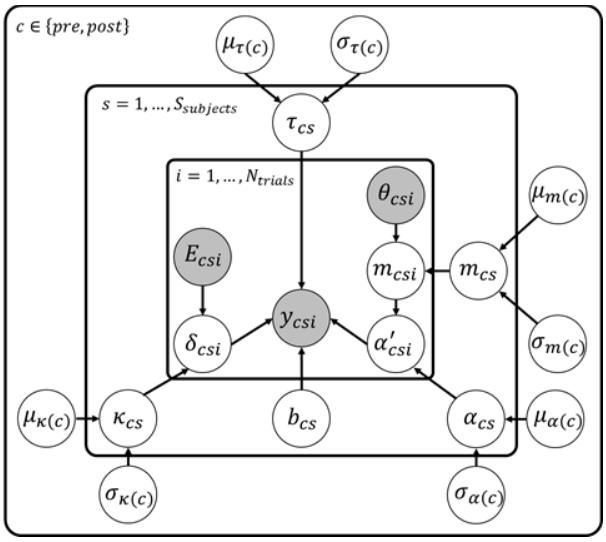

Model 1. SFS modulation of boundary

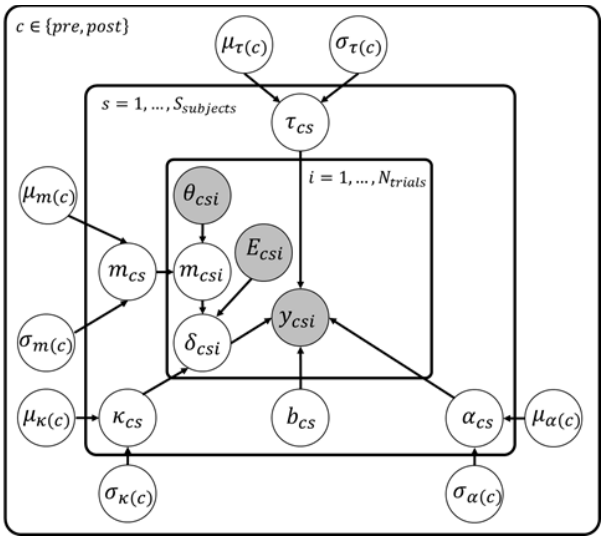

Model 2. SFS modulation of drift rate

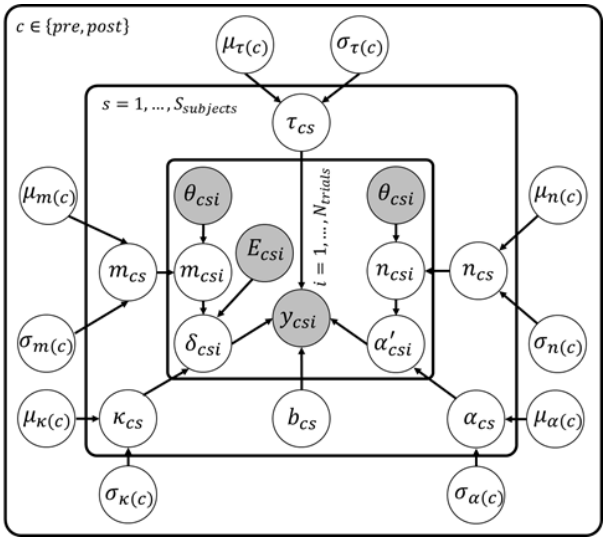

Model 3. Separate SFS Modulation of boundary and drift rate

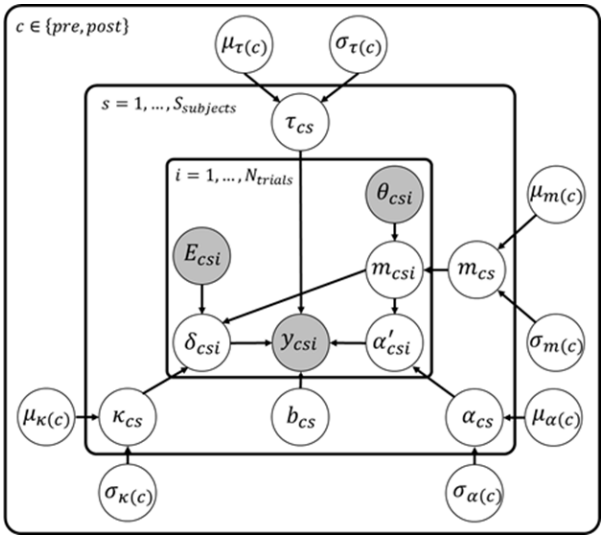

Model 4. Joint SFS modulation of both boundary and drift rate

Supplementary Figure 8. Neural-HDDM Alternatives. To test whether the left SFS is mechanistically involved in the latent decision-relevant processes, we included trial-by-trial left SFS neural betas as an input to our hierarchical drift diffusion model. We compared our neural HDDM with the HDDM without neural inputs. We additively incorporated trialwise left SFS and used a scale parameter, $m_{c,s}$, to account for its modulatory effects. The following equations show the distributions assumed for each of the latent variables in the model:

Trial-by-trial, i $\quad y_{c,s,i} \sim Wiener(\alpha_{c,s}, \beta, \tau_{c,s}, \delta_{c,s,i})$

Model 1: $\delta_{c,s,i} = \kappa_{c,s} \times E_{c,s,i}$
$\alpha_{c,s,i} = \alpha_{c,s} + \left(m_{c,s} \times \theta_{c,s,i}\right)$

Model 2: $\delta_{c,s,i} = \kappa_{c,s} \times E_{c,s,i} + \left(m_{c,s} \times \theta_{c,s,i}\right)$

Model 3: $\delta_{c,s,i} = \kappa_{c,s} \times E_{c,s,i} + \left(m_{c,s} \times \theta_{c,s,i}\right)$
$\alpha_{c,s,i} = \alpha_{c,s} + \left(n_{c,s} \times \theta_{c,s,i}\right)$

Model 4: $\delta_{c,s,i} = \kappa_{c,s} \times E_{c,s,i} + \left(m_{c,s} \times \theta_{c,s,i}\right)$
$\alpha_{c,s,i} = \alpha_{c,s} + (m_{c,s} \times \theta_{c,s,i})$

Subject, c

$\alpha_{c,s} \sim \mathbb{N}\left(\mu_{\alpha(c)}, \sigma^2_{\alpha(c)}\right)$

$\tau_{c,s} \sim \mathbb{N}\left(\mu_{\tau(c)}, \sigma^2_{\tau(c)}\right)$

$\kappa_{c,s} \sim \mathbb{N}\left(\mu_{\kappa(c)}, \sigma^2_{\kappa(c)}\right)$
$b_{c,s} = 0.5$
$m_{c,s} \sim \mathbb{N}\left(\mu_{m(c)}, \sigma^2_{m(c)}\right)$ (All Models)

$n_{c,s} \sim \mathbb{N}\left(\mu_{n(c)}, \sigma^2_{n(c)}\right)$ (Model 3 only)

Observable variables

$y = \begin{cases} rt\,, & correct = 1 \\ -rt, & correct = 0 \end{cases}$

$E = \{V_{best} - V_{worst}\}$ or $\{S_{biggest} - S_{smallest}\}$

θ, z-scored

Particularly, (**a) Model 1** incorporates trialwise left SFS betas into the decision boundary. **(b) Model 2** incorporates trialwise left SFS betas into the drift rate. **(c) Model 3** includes trial-by-trial betas in both decision thresholds and the drift rate, but with separate scale parameters. **(d) Model 4** includes trial-by-trial betas in both latent parameters but with one common scale parameter.

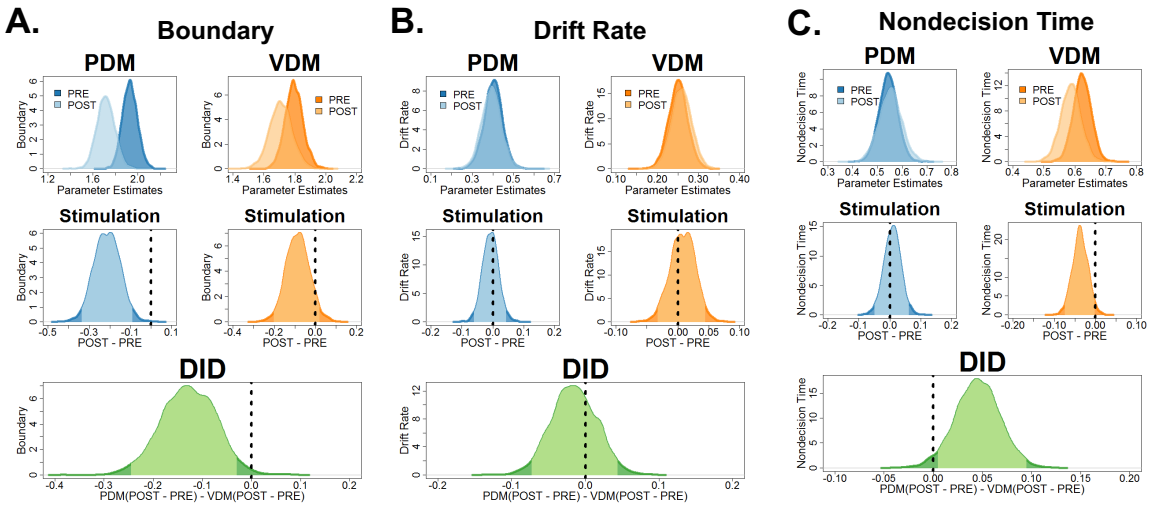

Supplementary Figure 9. Reanalysis of latent DDM parameters using the neural-HDDM confirmed the results of lower decision boundary in PDM and lower nondecision times in VDM. We used the winning neural-HDDM model where the left SFS is modulating the decision threshold (**Supplementary Fig. 8a**). **(a)** Bayesian posterior probability distributions (top row) of all DDM parameters show similar effects with the DDM without neural inputs. Post-hoc tests (middle and bottom rows) comparing pre-post perceptual decision making (PDM) differences with pre-post value-based decision making (VDM) differences show that theta-burst stimulation selectively reduced the decision boundary for perceptual, not value-based decisions. In particular, the criterion is well outside the 95% HDI. **(b)** The mean drift rate remained unaffected even with our neural-HDDM model (the criterion is within the 95% HDI). **(c)** Post-hoc tests also revealed lower nondecision times specifically for VDM, not PDM after stimulation (the criterion is outside the 95% HDI).

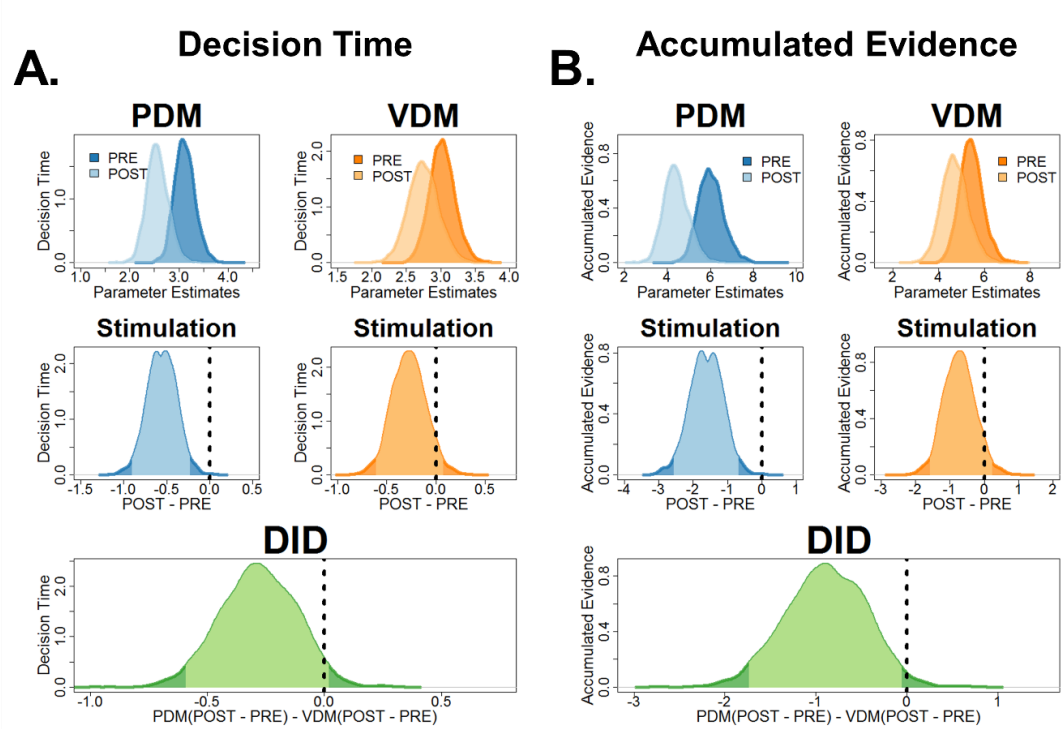

Supplementary Figure 10. Reanalysis of decision times and accumulated evidence using the neural-HDDM provide improvements in model evidence and clearer statistical inference. Using the winning neural-HDDM model (**Supplementary Fig. 8a**), we derived measures for **(a)** decision times and **(b)** accumulated evidence and tested whether improvements in model evidence reflect improvements in statistical inference. Post-hoc tests comparing pre-post PDM difference revealed a main stimulation effect in both DT and AE for PDM (middle row, criteria outside the 95% HDI). Further post-hoc analysis (bottom row) comparing the pre-post PDM difference with the pre-post VDM difference show that decision times are now marginally close to the border of the 95% HDI while accumulated evidence is now outside the 95% HDI.

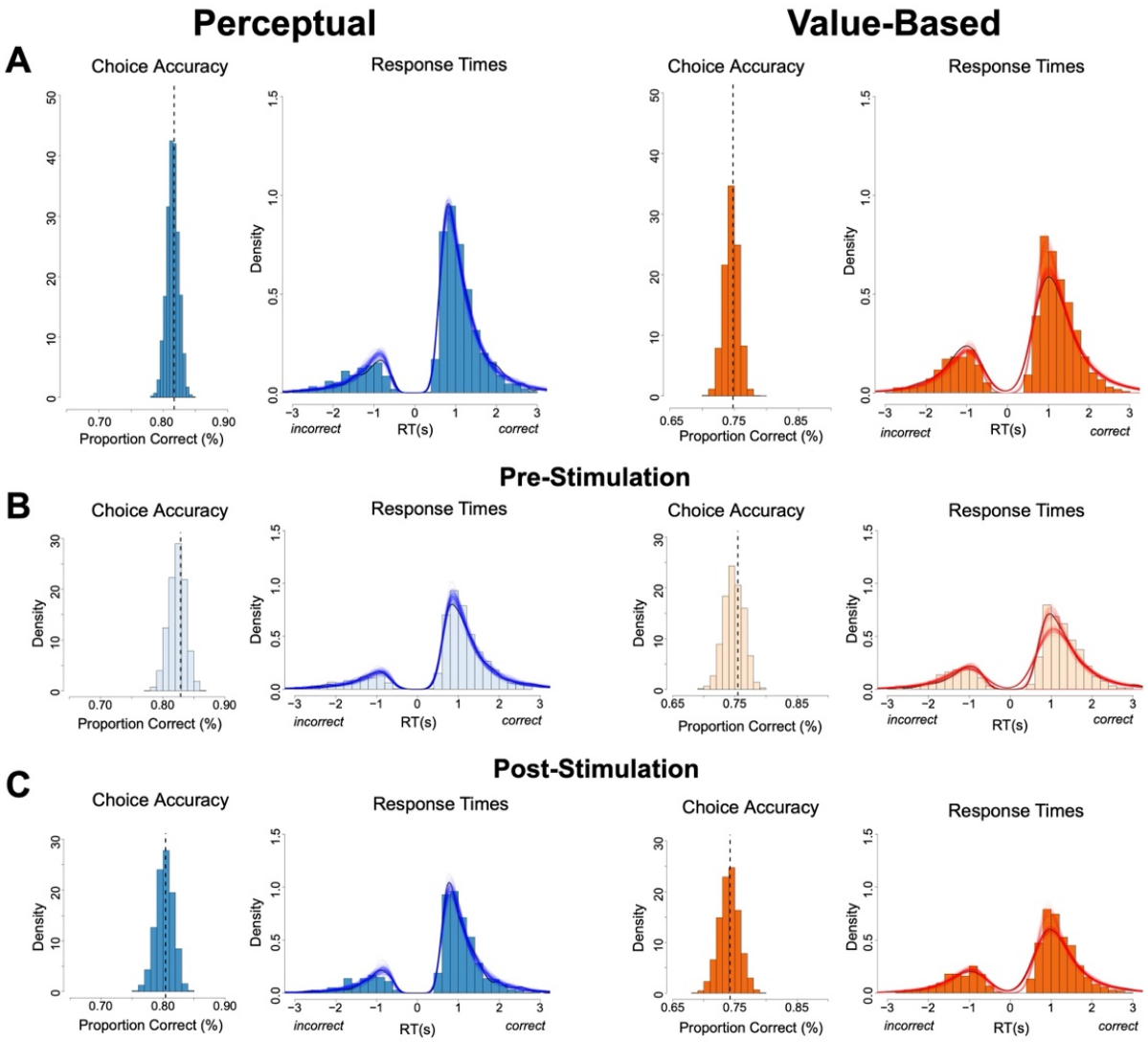

Supplementary Figure 11. Posterior predictive checks: overall accuracy and RT distributions. Posterior predictive simulations from the fitted HDDM compared to observed data. **Left column:** histograms show the simulated distribution **of** mean accuracy across 3,000 posterior draws; the vertical dashed line marks the observed mean accuracy. **Right column:** observed **RT histograms** (positive = correct; negative = error) with posterior predictive density curves overlaid. Panels show (a) PDM vs VDM (pooled over TMS), (b) pre-TMS, and (c) post-TMS**.** The model reproduces both accuracy and RT patterns in each condition.

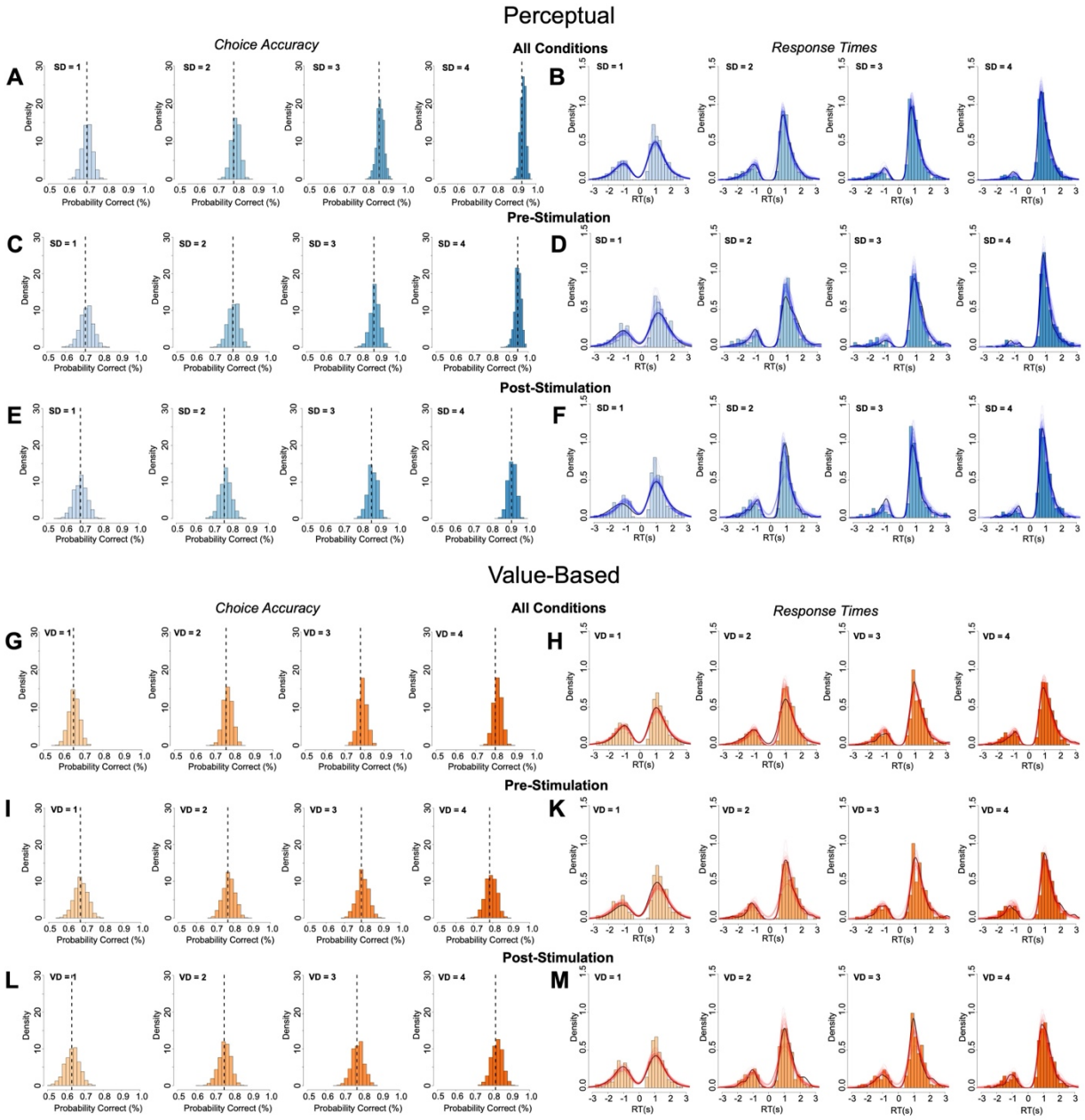

Supplementary Figure 12. Posterior predictive checks by evidence level. As in Response Figure 5, but split by evidence level 1–4 (left-to-right within each row). Rows display: (top) **PDM** pooled over TMS, (middle) **pre-TMS**, and (bottom) **post-TMS**; the corresponding three rows for **VDM** are arranged analogously. Simulations closely match accuracy and RT distributions at each evidence level in both tasks.

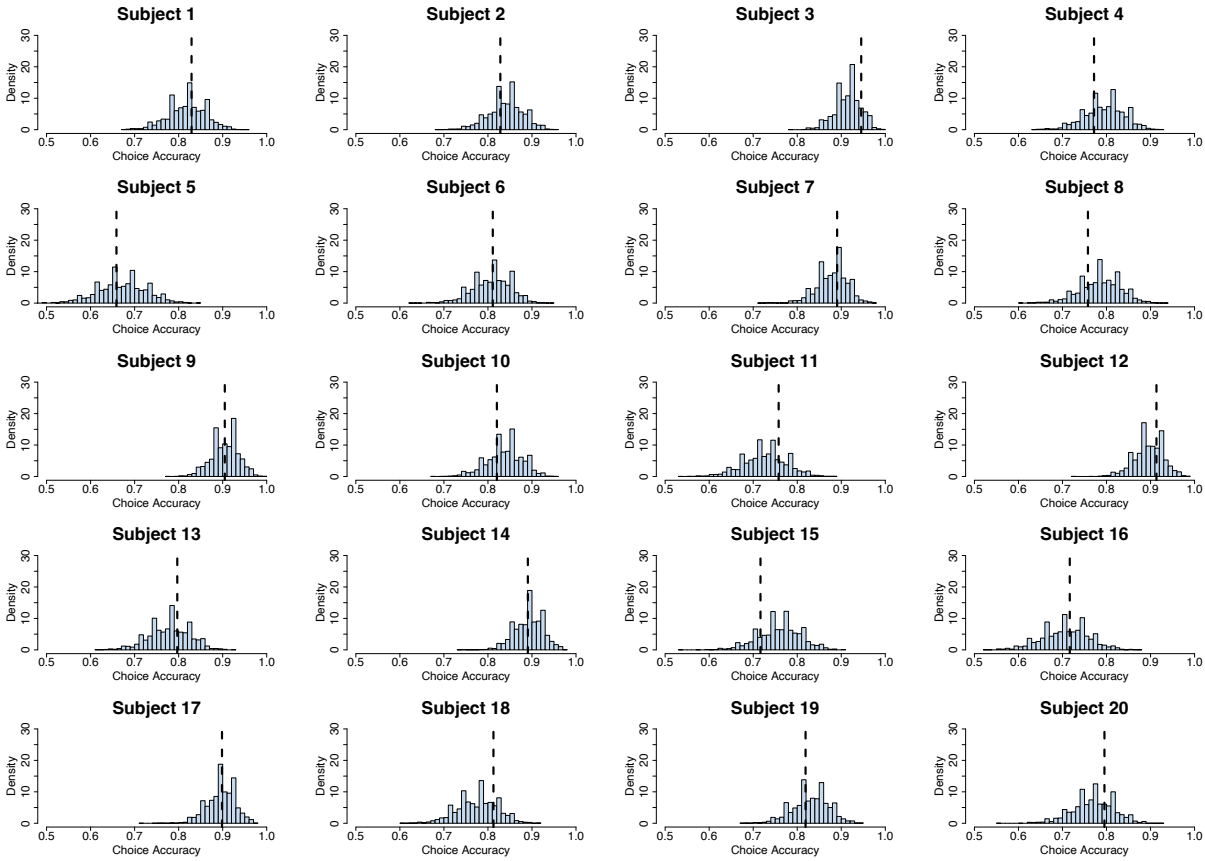

Supplementary Figure 13. Subject-level accuracy fits for PDM. For each participant, histogram shows the posterior predictive distribution of that participant's mean accuracy from 3,000 simulations; the **vertical dashed line** marks the observed mean accuracy for that participant. The HDDM captures the dispersion of accuracies across individuals in PDM.

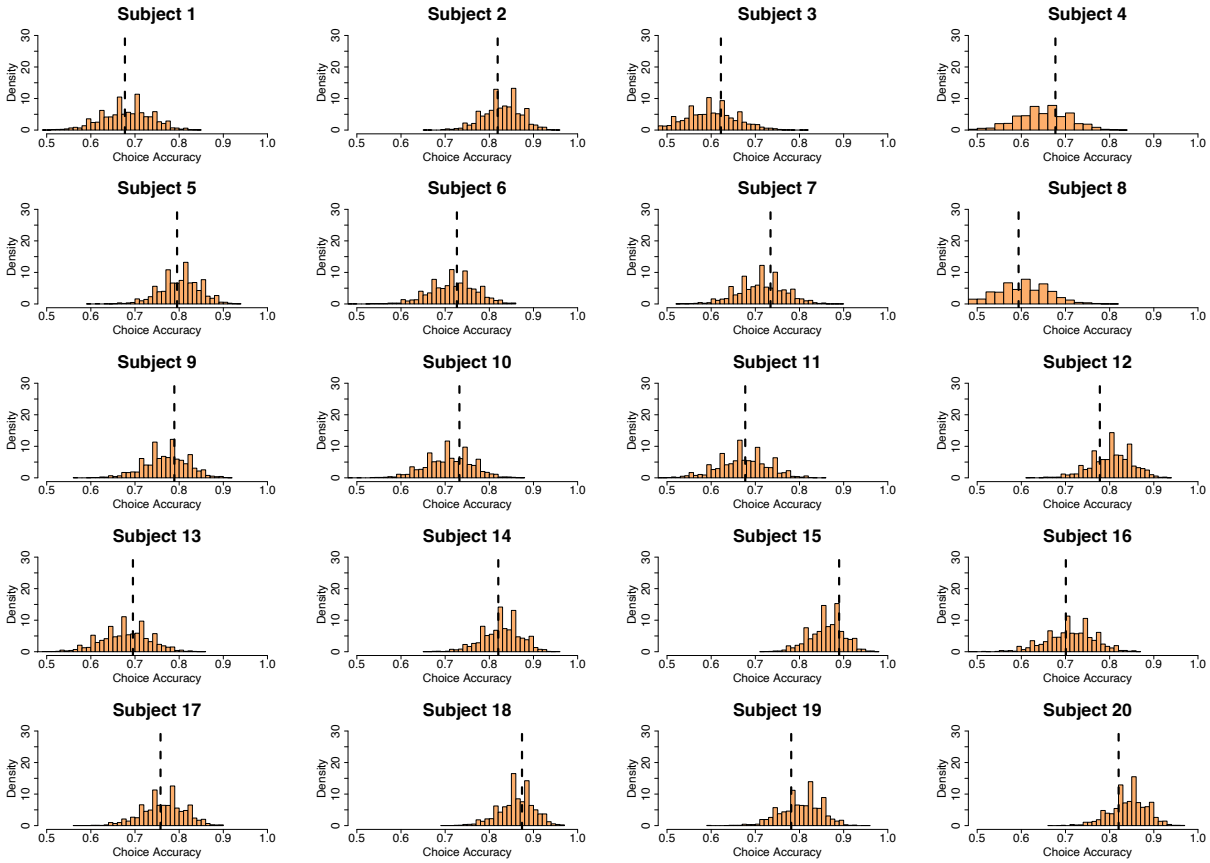

Supplementary Figure 14. Subject-level accuracy fits for VDM. Same format as Response Figure 7, for **VDM**. Posterior predictive distributions align with observed subject-level accuracies, indicating good recovery of between-subject variability in the value-based task.

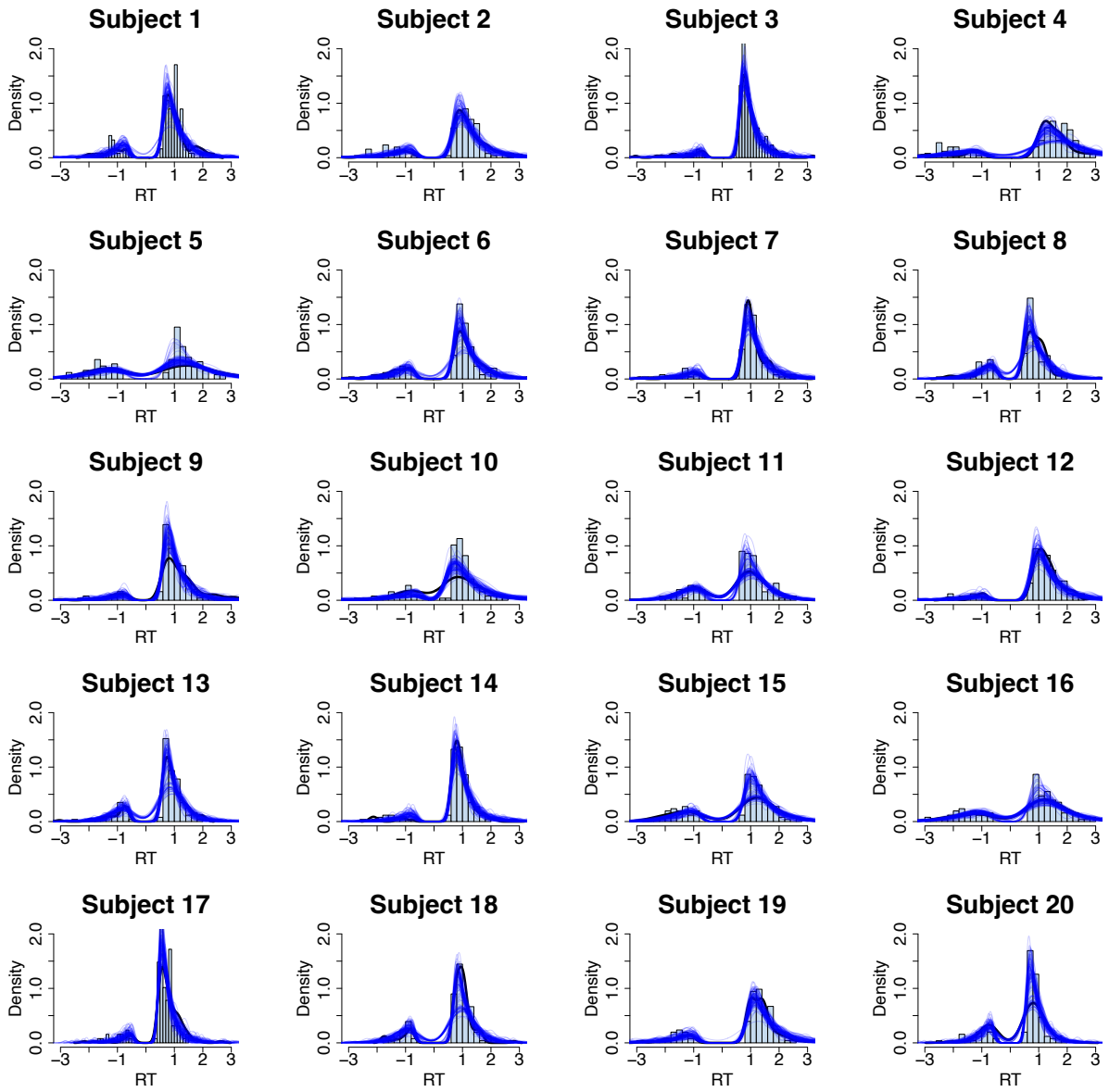

Supplementary Figure 15. Subject-level RT distribution fits for PDM. For each participant, observed PDM RT histograms (positive = correct; negative = error) are overlaid with posterior predictive density curves from the HDDM. The model reproduces the full shape of individual RT distributions, including correct/error asymmetries.

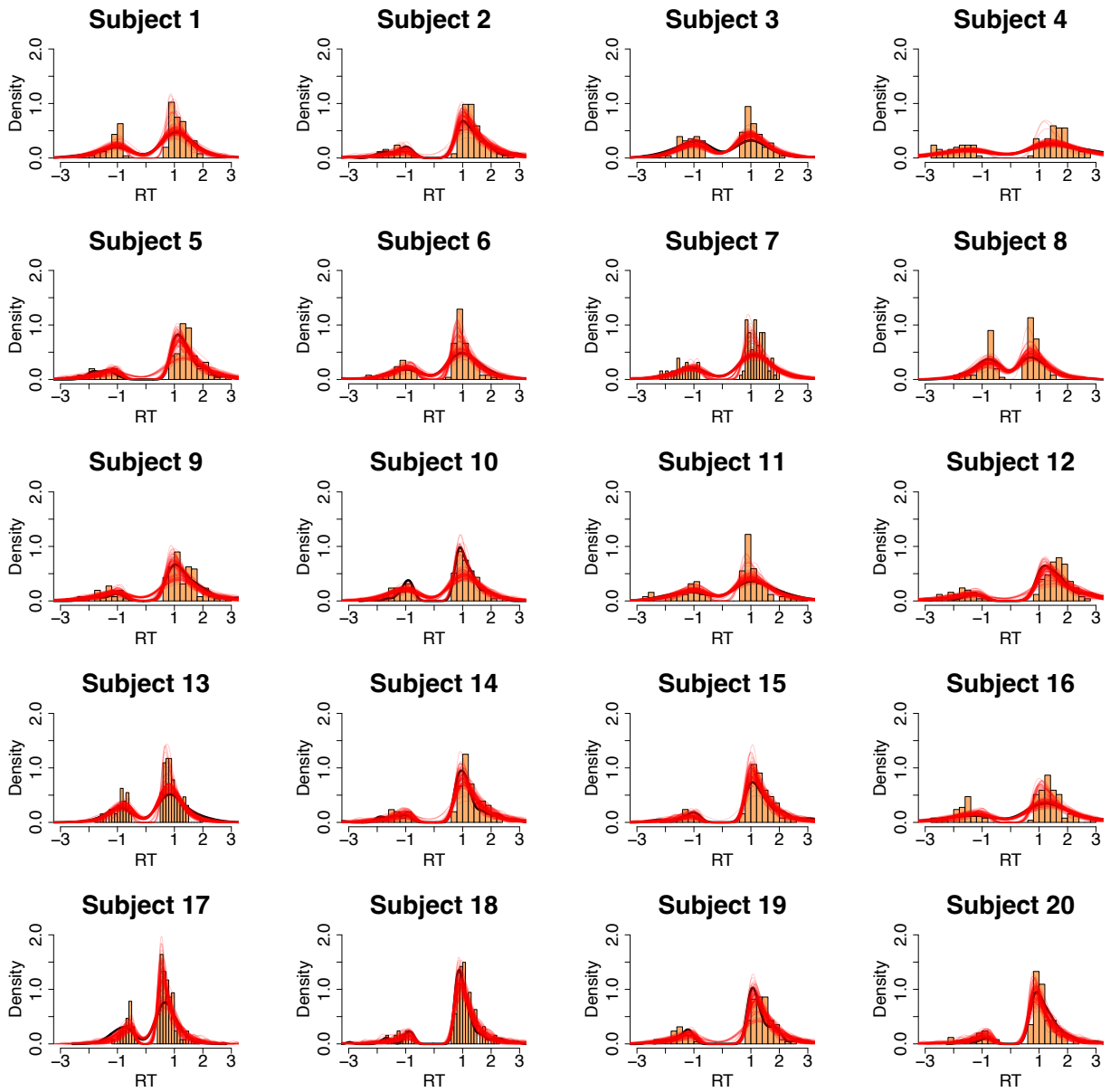

Supplementary Figure 16. Subject-level RT distribution fits for VDM. Same format as Response Figure 9, for **VDM**. Posterior predictive densities closely track the observed RT distributions across participants.

Supplementary Table 1.

Average brain activity that is common for both types of choice (conjunction between PDM and VDM trials)

Region	Peak-Side	Cluster Size	x	y	z	Z score	T score	p-value
Fusiform gyrus	L	1072	-33	-52	-17	Inf.	22.61	< 0.001
Fusiform gyrus	R	1523	33	-52	-11	7.23	17.24	< 0.001
Anterior intraparietal sulcus	L	845	-48	-34	46	7.13	16.53	< 0.001
Caudal supplementary motor	L	525	-3	14	49	7.05	15.98	< 0.001
Middle cingulate cortex	L	99	-6	-31	28	6.92	15.17	< 0.001
Anterior insula	L	219	-33	23	1	6.62	13.49	< 0.001
Hippocampus/Thalamus	R	42	21	-28	4	6.40	12.36	< 0.001
Hippocampus/Thalamus	L	483	-21	-31	1	6.35	12.11	< 0.001
Anterior insula	R	187	30	26	-2	6.18	11.36	< 0.001
Somatosensory	L	55	-36	-4	10	5.89	10.18	< 0.001
Cerebellum	R	32	0	-52	-35	5.69	9.45	< 0.001
Cerebellum	L	18	-9	-76	-26	5.33	8.29	< 0.001
Premotor cortex / Inferior frontal sulcus	R	25	51	8	28	5.32	8.25	< 0.001
Premotor cortex / Inferior frontal sulcus	L	33	-54	8	34	5.25	8.06	< 0.001
Cerebellum	R	3	9	-76	-38	5.16	7.80	0.004
Frontal eye field	R	19	24	-1	49	5.14	7.73	< 0.001
Cerebellum	L	4	-6	-79	-41	5.12	7.69	0.002
Medial temporal lobe	L	3	-27	-4	-32	5.12	7.68	0.004
Dorsolateral prefrontal	R	6	42	32	25	5.09	7.59	0.001
Cerebellum	R	5	15	-55	-47	5.03	7.44	0.001
Cerebellum	R	3	18	-67	-47	4.94	7.18	0.004
Cerebellum	R	1	9	-73	-23	4.86	6.99	0.015
Basal ganglia	L	4	-15	5	4	4.86	6.98	0.002
Frontal eye field	L	1	-30	-4	49	4.83	6.92	0.015
Supplementary motor cortex	L	2	-6	-4	61	4.83	6.92	0.007
Somatosensory cortex	L	1	-54	-19	19	4.82	6.88	0.015
Brainstem	R	1	9	-34	-32	4.80	6.85	0.015
Brainstem	R	1	0	-31	-38	4.80	6.85	0.015
Parietal cortex	L	1	-24	2	55	4.79	6.81	0.015

All p-values are FWE-corrected for the whole brain.

Supplementary Table 2.

Average brain activity that is distinct for both types of choice.

Region	Peak-Side	Cluster Size	x	y	Z	Z score	T score	p-value
Value-based choice trials > Perceptual choice trials								
Angular gyrus	L	344	-45	-70	43	5.74	9.62	< 0.001
Superior frontal	L	1560	-18	32	46	5.36	8.40	< 0.001
Temporal parietal junction	R	204	51	-61	37	4.71	6.62	< 0.001
Posterior cingulate cortex	L	1368	-3	-55	22	4.66	6.51	< 0.001
Cerebellum	R	171	39	-61	-47	4.62	6.41	< 0.001
Orbitofrontal cortex	L	130	-39	38	-11	5.31	8.24	< 0.001
Middle temporal gyrus	L	118	-63	-22	-20	4.40	5.90	0.002
Superior frontal	R	75	18	35	46	3.95	5.02	0.042
Medial prefrontal cortex	L	24	-9	50	1	4.02	5.14	0.027
Basal forebrain	L	11	-15	20	-14	3.57	4.33	0.011[SVC]
Superior temporal gyrus	L	1	-63	-22	-5	3.19	3.73	0.033 [SVC]
Perceptual choice trials > Value-based choice trials								
Frontal eye fields	R	79	24	-1	55	5.01	7.39	0.035
Premotor cortex	R	176	51	8	19	4.59	6.34	0.001
Intraparietal sulcus	R	646	39	-40	46	4.59	6.34	< 0.001
Inferior temporal sulcus	R	124	45	-55	1	4.36	6.82	0.005
Anterior parietal sulcus	L	319	-51	-31	40	4.29	5.67	< 0.001

All p-values are FWE-corrected for the whole brain. SVC = small-volume-correction.

Supplementary Table 3.

Regions encoding trialwise accumulated evidence (parametric modulation) during perceptual and value-based decisions, including SFS SVC results for both tasks.

Region	Peak-Side	Cluster Size	x	y	z	Z score	T score	p-value
Total Accumulation Value-based Decisions								
Lingual gyrus	L	1338	-9	-88	-2	5.83	9.98	< 0.001
Supplementary Motor Area	L	887	-6	-4	43	4.58	6.32	< 0.001
Primary Auditory Cortex	R	145	36	-31	16	4.53	6.19	< 0.001
Total Accumulation Perceptual Decisions								
Cuneus, V3	R	1215	0	-91	13	5.00	7.36	< 0.001
Lingual gyrus	R	1006	12	-76	-5	4.87	7.01	< 0.001
Superior frontal sulcus*	L	1	-21	26	37	3.13	3.64	0.039^{SVC}
Total Accumulation Value-based ∩ Perceptual Decisions								
Cuneus, V3	R	1528	6	-88	10	6.99	15.60	< 0.001
Postcentral gyrus	R	316	6	-49	73	4.31	7.73	< 0.001
Lingual gyrus*	L	518	-9	-91	1	4.38	5.98	< 0.001
Total Accumulation Value-based > Perceptual Decisions								
Nucleus Accumbens	R	395	9	11	-11	3.92	4.94	< 0.001
Supramarginal gyrus	L	166	-63	-28	37	3.42	4.09	0.023
Ventromedial prefrontal cortex*	L	2	0	38	-14	3.16	3.68	0.032^{SVC}

Note: Trialwise AE during both types of choices correlated negatively with BOLD activity in intraparietal sulcus (IPS) (peak at $x = -33, y = -49, z = 58$; $SVC < 0.05$; Supplementary Fig. 7c) and bilateral fusiform gyrus (right peak at $x = 33, y = -49, z = -14$; left peak at $x = -30, y = -52, z = -11$; FWE-corrected with cluster-forming thresholds at $T(19) > 2.9$; Supplementary Fig. 7c). Note that the inverse of total evidence is directly proportional to the efficiency of evidence accumulation (see **Methods** for more details). SVC = small-volume-correction.

1535 **Supplementary Table 4.**

1536 Average brain activity that represents efficiency of evidence accumulation for both types of choice

1537

Region	Peak-Side	Cluster Size	x	y	z	Z score	T score	p-value
Accumulation Rate for Value-based Decisions								
Fusiform gyrus	R	564	33	-55	-11	4.92	7.15	< 0.001
Fusiform gyrus	L	718	-27	-70	-11	4.92	7.14	< 0.001
Occipital	R	349	30	-85	10	3.75	4.65	< 0.001
Intraparietal sulcus	L	58	-28	-66	38	4.35	5.80	0.002^{SVC}
Intraparietal sulcus	R	19	27	-61	43	3.52	4.25	0.032^{SVC}
Accumulation Rate for Perceptual Decisions								
Fusiform gyrus	L	1095	-24	-82	-8	5.72	9.56	< 0.001
Fusiform gyrus	R	1250	33	-55	-11	5.06	7.51	< 0.001
Intraparietal sulcus	R	58	27	-61	43	3.54	4.29	0.009^{SVC}
Accumulation Rate for Value-based ∩ Perceptual Decisions								
Fusiform gyrus	L	1151	-24	-82	-8	5.75	9.69	< 0.001
Fusiform gyrus	R	1369	33	-55	-11	5.47	8.73	< 0.001
Intraparietal sulcus	R	81	27	-61	43	3.66	4.49	0.003^{SVC}

1538 SVC = small-volume-correction.

1539

Supplementary Table 5.

Differences-in-differences results for choice accuracy/consistency and response times

	Perceptual		Value-Based	
	(a)	(b)	(c)	(d)
Accuracy				
(1) active DV	0.5596***	0.5178***	0.249***	0.245***
	(0.053)	(0.047)	(0.061)	(0.062)
(2) passive DV	0.0232	0.0258	0.006	0.005
	(0.178)	(0.015)	(0.026)	(0.027)
(3) active overall value (OV)	–0.2023***	–0.210***	0.088	0.073
	(0.041)	(0.046)	(0.151)	(0.057)
(4) passive OV	–0.060	–0.048	–0.027	–0.027
	(0.060)	(0.060)	(0.063)	(0.063)
(5) RTs		–1.0679***		–0.254
		(0.160)		(0.165)
(6) Constant	0.720***	2.131***	0.200	0.569
	(0.221)	(0.301)	(0.239)	(0.293)
RTs				
(1) active DV	–0.058***	–0.041***	–0.016*	–0.013*
	(0.007)	(0.007)	(0.033)	(0.006)
(2) passive DV	0.002	0.002	–0.003	–0.003
	(0.002)	(0.002)	(0.004)	(0.003)
(3) active OV	–0.002	–0.008	–0.057***	–0.056***
	(0.007)	(0.007)	(0.004)	(0.007)
(4) passive OV	0.011	0.009	0.006	0.006
	(0.007)	(0.007)	(0.007)	(0.006)
(5) Choice response		–0.220***		–0.080***
		(0.020)		(0.017)
(7) Constant	1.289	1.442	1.431	0.010
	(0.0623)	(0.062)	(0.060)	(0.035)
Total Observations	2,544	2,548	2,544	2,548
Sessions	8	8	8	8
Subjects	20	20	20	20

Significance: * $p < 0.05$, ** $p < 0.01$

Supplementary Table 6.

Differences-in-differences results for choice accuracy/consistency and response times

	(a) Pre-Post cTBS	(b) + Training	(c) + Control Variables	(d) + Training & Control Variables
Accuracy				
(1) Perceptual	–0.433*	–0.465**	–0.459*	–0.484**
	(0.188)	(0.174)	(0.192)	(0.180)
(2) Value-based	0.00298	–0.0415	0.0042	–0.040
	(0.124)	(0.104)	(0.123)	(0.104)
(3) DD Estimate	–0.293*	–0.273*	–0.319**	–0.288*
	(0.114)	(0.135)	(0.115)	(0.136)
(4) Corrected	–0.075**	–0.094*	–0.087**	–0.103*
	(0.027)	(0.045)	(0.030)	(0.047)
RTs				
(1) Perceptual	–0.090*	–0.116**	–0.089*	–0.125**
	(0.0331)	(0.0343)	(0.033)	(0.033)
(2) Value-based	–0.117**	–0.125**	–0.117**	–0.125**
	(0.0298)	(0.0328)	(0.030)	(0.033)
(3) DD Estimate	0.0265	0.00929	0.0273	0.010
	(0.0357)	(0.0353)	(0.035)	(0.035)
Perceptual Obs.	1,272	1,907	1,272	1,907
Value-based Obs.	1,276	1,908	1,276	1,908
Total Obs.	2,548	3,815	2,548	3,815
Sessions	4	6	4	6
Subjects	20	20	20	20

Significance: * $p < 0.05$, ** $p < 0.01$

Note:

(a) **Pre-Post cTBS:** Stimulation effect comparing the last two runs during pre-cTBS and the first two runs during post-cTBS.
(b) **Pre-Post cTBS + Training:** Stimulation effect comparing all runs during pre-cTBS with the first two runs during post-cTBS.
(c) **Pre-Post cTBS + Control Variables:** The same as in (a) but we added control variables to test for robustness of the stimulation effect.
(d) **Pre-Post cTBS + Training + Control Variables:** The same as in (b) but we added control variables to test for robustness of the stimulation effect.

Supplementary Table 7.

Differences-in-differences results for choice accuracy/consistency and response times

	(a) Pre-Post cTBS	(b) + Training	(c) + Control Variables	(d) + Training & Control Variables
Accuracy				
(1) PDM SFS x Stimulation	–0.145**	–0.133**	–0.195**	–0.318**
	(0.047)	(0.043)	(0.057)	(0.106)
(2) VDM SFS x Stimulation	0.148	0.104	0.167	–0.065
	(0.084)	(0.080)	(0.090)	(0.053)
(3) SFS x Stimulation x Task	–0.293**	–0.237**	–0.356**	–0.318**
	(0.101)	(0.088)	(0.121)	(0.103)
(4) Corrected Triple Interaction	–0.086*	–0.093*	–0.102*	–0.131**
	(0.034)	(0.038)	(0.040)	(0.047)
RTs				
(1) PDM SFS x Stimulation	–0.003	–0.005	–0.009	–0.005
	(0.0140)	(0.0148)	(0.0137)	(0.0142)
(2) VDM SFS x Stimulation	–0.003	0.011	–0.003	0.008
	(0.0227)	(0.0182)	(0.0232)	(0.0182)
(3) SFS x Stimulation x Task	–0.0002	–0.016	–0.018	–0.012
	(0.0273)	(0.0241)	(0.0240)	(0.0238)
Perceptual Obs.	1,272	1,907	1,272	1,907
Value-based Obs.	1,276	1,908	1,276	1,908
Total Obs.	2,548	3,815	2,548	3,815
Sessions	4	6	4	6
Subjects	20	20	20	20

Significance: * $p < 0.05$, ** $p < 0.01$

Note:

(a) **Pre-Post cTBS:** Stimulation effect comparing the last two runs during pre-cTBS and the first two runs during post-cTBS.
(b) **Pre-Post cTBS + Training:** Stimulation effect comparing all runs during pre-cTBS with the first two runs during post-cTBS.
(c) **Pre-Post cTBS + Control Variables:** The same as in (a) but we added control variables to test for robustness of the stimulation effect.
(d) **Pre-Post cTBS + Training + Control Variables:** The same as in (b) but we added control variables to test for robustness of the stimulation effect.

Supplementary Table 8. HDDM group-level parameter estimates for perceptual decisions **(PDM)** across TMS conditions and evidence levels (δ drift, α boundary, τ non-decision time; DIC reported).

	δ		α		τ		
Perceptual	mean	SD	mean	SD	mean	SD	DIC
All	0.388	0.035	1.848	0.065	0.522	0.029	4048.675
Pre-stimulation	0.401	0.041	1.915	0.078	0.537	0.035	2103.361
Post-stimulation	0.394	0.039	1.708	0.070	0.545	0.023	1811.714
Evidence Level (all)							
1	0.502	0.075	1.755	0.071	0.565	0.038	1443.749
2	0.847	0.108	1.734	0.062	0.576	0.029	1111.493
3	1.176	0.126	1.824	0.076	0.530	0.030	898.764
4	1.570	0.143	1.945	0.089	0.523	0.027	599.467
Evidence Level (pre-stimulation)							
1	0.521	0.083	1.815	0.088	0.571	0.043	785.636
2	0.907	0.122	1.738	0.080	0.633	0.044	576.199
3	1.211	0.159	1.908	0.096	0.533	0.036	494.364
4	1.673	0.183	2.070	0.116	0.542	0.036	324.876
Evidence Level (post-stimulation)							
1	0.516	0.110	1.634	0.086	0.596	0.036	675.095
2	0.865	0.164	1.651	0.089	0.573	0.027	520.592
3	1.207	0.150	1.720	0.097	0.547	0.031	429.265
4	1.512	0.144	1.764	0.110	0.537	0.031	295.764

Supplementary Table 9. HDDM group-level parameter estimates for value-based decisions **(VDM)** across TMS conditions and evidence levels (δ, α, τ; DIC reported).

	δ		α		τ		
Value-Based	mean	SD	mean	SD	mean	SD	DIC
All	0.217	0.020	1.799	0.057	0.579	0.029	4960.166
Pre-stimulation	0.219	0.021	1.798	0.062	0.627	0.033	2523.472
Post-stimulation	0.222	0.022	1.707	0.066	0.585	0.031	2305.875
Evidence Level (all)							
1	0.386	0.054	1.680	0.064	0.616	0.033	1415.309
2	0.717	0.076	1.882	0.062	0.604	0.035	1274.095
3	0.806	0.088	1.748	0.076	0.618	0.038	1153.058
4	0.888	0.111	1.849	0.079	0.579	0.031	1135.478
Evidence Level (pre-stimulation)							
1	0.453	0.086	1.682	0.060	0.690	0.052	724.036
2	0.726	0.084	1.756	0.080	0.660	0.033	655.603
3	0.838	0.096	1.707	0.083	0.675	0.044	585.722
4	0.848	0.134	1.798	0.083	0.639	0.037	604.951
Evidence Level (post-stimulation)							
1	0.350	0.078	1.585	0.077	0.620	0.038	675.120
2	0.737	0.111	1.631	0.072	0.627	0.043	590.912
3	0.818	0.128	1.619	0.094	0.650	0.048	544.877
4	0.960	0.109	1.721	0.085	0.609	0.044	538.493

Supplementary Table 10. HDDM participant-level parameter estimates for **PDM (δ, α, τ)** with model fit (DIC) per subject.

	δ		α		τ		
Subject	mean	SD	mean	SD	mean	SD	DIC
1	0.416	0.050	1.654	0.086	0.498	0.014	155.658
2	0.378	0.042	2.034	0.104	0.510	0.020	246.230
3	0.668	0.057	1.846	0.120	0.487	0.017	75.702
4	0.257	0.034	2.336	0.112	0.742	0.026	355.873
5	0.147	0.034	2.026	0.086	0.587	0.018	346.635
6	0.358	0.044	1.796	0.086	0.567	0.015	207.893
7	0.504	0.050	1.932	0.109	0.565	0.018	164.511
8	0.338	0.047	1.678	0.075	0.357	0.012	194.419
9	0.571	0.052	2.026	0.120	0.446	0.018	152.084
10	0.330	0.038	2.296	0.116	0.222	0.017	283.846
11	0.252	0.042	1.649	0.075	0.547	0.017	242.651
12	0.482	0.045	2.248	0.135	0.555	0.021	201.924
13	0.361	0.049	1.532	0.071	0.484	0.011	151.426
14	0.578	0.055	1.823	0.106	0.494	0.016	121.826
15	0.271	0.041	1.835	0.083	0.656	0.017	263.821
16	0.189	0.035	1.969	0.086	0.551	0.021	333.834
17	0.676	0.065	1.597	0.088	0.345	0.010	36.774
18	0.359	0.048	1.516	0.072	0.592	0.012	146.552
19	0.360	0.041	2.016	0.101	0.728	0.017	247.041
20	0.375	0.055	1.406	0.067	0.490	0.012	129.653

Supplementary Table 11. HDDM **participant-level** parameter estimates for **VDM** (δ, α, τ) with model fit (DIC) per subject.

	δ		α		τ		
Subject	mean	SD	mean	SD	mean	SD	DIC
1	0.165	0.037	1.582	0.067	0.612	0.012	224.450
2	0.280	0.034	2.076	0.103	0.606	0.017	256.215
3	0.085	0.035	1.610	0.068	0.526	0.015	271.958
4	0.097	0.028	2.158	0.091	0.684	0.023	394.165
5	0.257	0.034	1.961	0.096	0.721	0.020	270.684
6	0.198	0.035	1.646	0.074	0.518	0.015	239.416
7	0.187	0.036	1.680	0.074	0.642	0.013	242.186
8	0.090	0.038	1.559	0.064	0.330	0.011	235.979
9	0.220	0.033	1.950	0.093	0.560	0.021	298.440
10	0.184	0.036	1.667	0.075	0.584	0.016	254.361
11	0.137	0.032	1.794	0.078	0.479	0.016	297.167
12	0.226	0.030	2.236	0.109	0.735	0.021	317.836
13	0.185	0.042	1.389	0.060	0.483	0.011	173.978
14	0.291	0.036	1.963	0.094	0.580	0.016	243.953
15	0.342	0.037	1.997	0.106	0.663	0.018	206.759
16	0.160	0.032	1.964	0.084	0.643	0.017	315.890
17	0.288	0.048	1.431	0.062	0.338	0.008	125.692
18	0.379	0.041	1.805	0.097	0.592	0.016	155.570
19	0.273	0.035	1.853	0.088	0.759	0.015	235.053
20	0.331	0.038	1.871	0.093	0.516	0.015	201.545